Chapter 3

ORDER PARAMETER FLUCTUATIONS: OPF PARAMETERS

1. Self-averaging in spin glasses

In disordered systems any physical quantity X has, in general, a different value for every realisation of the quenched disorder. Thus, it is a random variable described by a distribution function $\mathcal{P}(\mathrm{X})$. This distribution function may be characterised by its moments: the average $\overline{\mathrm{X}}$ and the variance $\Delta^2\mathrm{X} \equiv \overline{\mathrm{X}^2} - \overline{\mathrm{X}}^2$. The self-averaging hypothesis states that any macroscopic thermodynamic quantity X is such that the relative fluctuations $\mathcal{R}_\mathrm{X}$ vanish in the thermodynamic limit,

$$\mathcal{R}_\mathrm{X} \equiv \frac{\overline{\mathrm{X}^2} - \overline{\mathrm{X}}^2}{\overline{\mathrm{X}}^2} \sim \frac{1}{V} \overset{V\to\infty}{\to} 0 \quad . \tag{3.1}$$

The validity of this assumption implies that, in the thermodynamic limit, any intensive quantity $\mathrm{x} \equiv \frac{\mathrm{X}}{V}$ does not depend on the realisation of the quenched disorder. Hence, the value of x corresponding to a single sample coincides with that obtained from averaging over many samples. The legitimacy of such a statement is supported by experimental observations because these do not show any difference between different samples.

We have already pointed out in Sec. 2.2.2 that Brout proved that in systems with short-ranged interactions the free-energy is self-averaging (hereafter referred to as SA), hence any observable that can be computed from finite derivatives of the free-energy is SA too. However, Brout's argument fails when the quantities under study depend on the boundary conditions and also at a critical point where there are strong fluctuations and the correlation length ξ diverges. In critical spin systems with disorder whose behaviour

is described by the random fixed point [1] it can be shown that when $L \gg \xi$ there is SA but that for $L \ll \xi$ there is no SA and $\mathcal{R}_{\rm X}$ is a *universal* constant [AH96] [2]. This result is striking but has been proved to be valid in diluted ferromagnets and Ashkin-Teller models [WD95, WD98].

In spin-glasses all quantities which are measurable experimentally are SA. However, this is not the case of the order parameter because, in general, the $P(q)$ cannot be expressed in terms of the free-energy and its derivatives. In the paramagnetic phase, the probability distribution of the overlap is trivial in the thermodynamic limit: $P(q) = \delta(q)$. Hence the overlap is SA, which means that in a finite system it is a random variable distributed around its mean value with variance $\sigma^2 \propto 1/V$. Below T_c the overlap is a random variable that takes a different value different in every sample, with a mean different from zero. From MFT we know that the order parameter exhibits strong sample-to-sample fluctuations below T_c. The $P(q)$ is a non-trivial function of q, such that $P(q_{12}, q_{34}) \neq P(q_{12})P(q_{34})$. This is a direct consequence of the fact that at the transition, besides time reversal symmetry, replica symmetry is broken. However, this is not the case in the scaling theory of droplets. Within this picture only TRS breaks at the transition. Below T_c, q can only take two different values, $q = \pm q_{\rm EA}$ so that, in the thermodynamic limit, $P(q)$ is trivial and the fluctuations of the overlap vanish.

Analytic approaches have failed to make any insight in what is the real nature of the low-temperature phase of short ranged spin-glasses, and in particular on whether the ground state is droplet or MF like. The numerical approach is the only one that can shed any light on this issue. In this respect, the choice of the observables under study is crucial to obtain relevant information below T_c. Here we propose the study of parameters measuring order-parameter-fluctuations (OPF). The interest of measuring OPF is twofold, first because by defining the adequate parameters one can properly characterise the transition into the frozen phase of any spin/glass model. And second, because from the behaviour of OPF at low temperatures we can learn about the typical excitations relevant for the thermodynamics.

1.1 Parameters measuring OPF

A good numerical tool to study second order transitions from a disordered phase to an ordered one are adimensional parameters $\mathrm{P}(T, L)$, where T is the temperature and L the linear size of the system ($V = L^d$). Curves for different system sizes are expected to cross at the transition and satisfy the finite-size scaling ansatz [Car96, Bar83],

$$\mathrm{P}(L, T) = f\left((T - T_c(L))\, L^{\frac{1}{\nu_{\rm P}}} \right) \; ; \; T_c(L) = T_c(\infty) + a L^{-\frac{1}{\nu_{\rm P}}}, \qquad (3.2)$$

[1] We refer to systems in which disorder is a relevant perturbation. According to Harry's criterion this happens for dimension $d > 2$ [Car96]. Systems with lower dimensionality are described by the pure (P) fixed point, even though the introduction of disorder results in a shift of the critical temperature.

[2] In systems described by the pure fixed point there is *weak* self-averaging, meaning that $\mathcal{R}_{\rm X}$ vanishes as $\sim V^{-\alpha}$ with $0 < \alpha < d$.

where, usually, ν_P is the correlation length exponent and $T_c(\infty)$ is the critical temperature in the thermodynamic limit. Therefore, from the study of these quantities one can obtain the critical temperature as well as the correlation length exponent.

The Binder ratio, B_m[3], is very useful in ordered systems. This parameter measures the kurtosis of the distribution of the order parameter, that in ferromagnets is the average local magnetisation m,

$$B_m = \frac{1}{2}\left(3 - \frac{\langle m^4\rangle}{\langle m^2\rangle^2}\right) \; ; \qquad m = \frac{1}{V}\sum_i m_i \;\; . \tag{3.3}$$

In the high temperature PM phase m is a Gaussian distributed variable around zero with variance $\sigma^2 = 1/V$. Thereby, in the thermodynamic limit $\langle m^4\rangle = 3\,\langle m^2\rangle^2$ which yields $B_m = 0$. In the absence of a magnetic field, TRS is spontaneously broken at T_c, so that in the ordered phase m can take two values $\pm m_0(T)$ with equal probability. Hence, in the thermodynamic limit we have that $\langle m^4\rangle = \langle m^2\rangle^2$ and $B = 1$. The behaviour of the Binder parameter is thus very simple in the limit $V \to \infty$: $B = \Theta(T_c - T)$ as we schematise in Fig. 3.1.

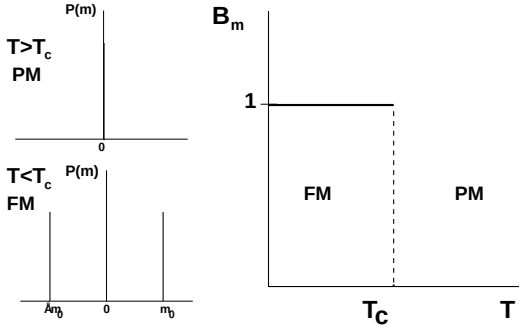

Figure 3.1. Binder cumulant for a ferromagnet, B_m, as defined in (3.3). On the right we plot B_m versus temperature in the absence of magnetic field. On the left we show the distribution of the order parameter m in the thermodynamic limit in the paramagnetic (PM) and ferromagnetic (FM) phases.

In spin glasses the Binder cumulant can be defined in terms of the overlap q as follows,

$$B = \frac{1}{2}\left(3 - \frac{\overline{\langle q^4\rangle}}{\overline{\langle q^2\rangle}^2}\right) \;\; . \tag{3.4}$$

where $\langle ...\rangle$ and $\overline{(...)}$ stand for thermal and disorder averages respectively. However, in spin glasses this parameter is not as useful as in ferromagnets. In systems containing time-reversal symmetry (TRS) in the Hamiltonian, B can be used successfully to determine

[3]We have introduced the subindex m to distinguish it from the Binder cumulant for spin glasses that we will denote as B.

the transition, *e.g.* in the SK model with no applied field (see Fig. 3.2). Nevertheless, its behaviour in the thermodynamic limit is not so simple as in ferromagnets. In the PM phase B vanishes as well but, below T_c, it becomes a non-trivial function of the temperature, even though at $T = 0$ it takes the universal value 1 because the ground state is unique [4]). Only within the droplet picture one recovers the trivial behaviour in the thermodynamic limit $B = \Theta(T_c - T)$. However, the Binder ratio does not work in models with a RSB transition but with no TRS in their Hamiltonian. In these cases, the Binder parameter can even become negative as is shown for the 3-state Potts model in Fig. 3.2.

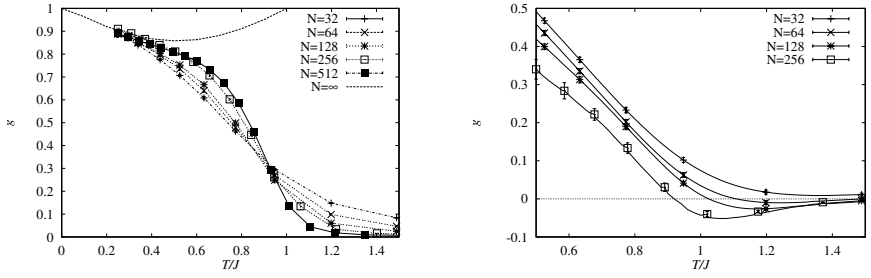

Figure 3.2. Binder cumulant for spin-glass models with and without TRS obtained from [HK00a]. *Left:* SK model with $h = 0$ (with TRS). *Right:* Potts model with three states (without TRS).

In models where RS is broken, the difference between the the PM phase and the SG is manifested in the lack of SA in the fluctuations of the order parameter below T_c. This phenomenon motivated the introduction of a new class of parameters measuring order-parameter fluctuations: G and A, that are defined as follows [MNP$^+$98a, BBDM98, MNP$^+$98b, PPR99],

$$G = \frac{\overline{\langle q^2\rangle^2} - \overline{\langle q^2\rangle}^2}{\overline{\langle q^4\rangle} - \overline{\langle q^2\rangle}^2} , \tag{3.5}$$

$$A = \frac{\overline{\langle q^2\rangle^2} - \overline{\langle q^2\rangle}^2}{\overline{\langle q^2\rangle}^2} . \tag{3.6}$$

The Binder cumulant bears the following relation with G and A, $B = 1 - \frac{1}{2}\frac{A}{G}$.

The strong sample-to-sample fluctuations existent in the thermodynamic limit of mean-field models can be formally expressed in terms of sum rules between the probability distribution of several overlaps. These can be easily derived using the replica equivalence property as is explained in Sec. 2.1. The existence of such relations inspired the definition

[4]Note that this is only true if couplings are continuously distributed.

of G with the aim of finding a parameter playing in spin glasses the same role that B plays in ordered systems. In particular, for the distribution of two overlaps we have the following identity,

$$P(q_{12}, q_{34}) = \frac{1}{3}P(q_{12})\delta(q_{12} - q_{34}) + \frac{2}{3}P(q_{12})P(q_{34}) \quad . \tag{3.7}$$

Multiplying each term in the identity by $q_{12}^2 q_{34}^2$ and integrating for all $q_{12},\ q_{34}$ we obtain the following relation between the moments of the overlap,

$$\overline{\langle q^2 \rangle^2} = \frac{1}{3}\overline{\langle q^4 \rangle} + \frac{2}{3}\overline{\langle q^2 \rangle}^2 \quad . \tag{3.8}$$

Introducing relation (3.8) in (3.5) yields that $G = 1/3$ below T_c. Hence, for mean-field models, G displays a trivial behaviour in the thermodynamic limit,

$$G = \frac{1}{3}\Theta(T_c - T) \quad . \tag{3.9}$$

The validity of RE beyond mean field is not assured. Nonetheless, these sum rules were rederived by Guerra [Gue96] for any disordered system provided it were stochastically stable in the presence of a mean-field perturbation, suggesting the validity of such relations also in finite-dimensional systems [5]. Based on these grounds, we put forward the conjecture that in the thermodynamic limit $G = 1/3$ below the critical temperature in any spin glass system, regardless of whether OPF are finite or not. Numerical simulations support such a conjecture. Note that G may remain finite even in replica symmetric phases with $q_{\rm EA} \neq 0$ where OPF vanish as $\sim 1/V^{\alpha}$ with $\alpha > 1$, but that it vanishes in the paramagnetic phase where the order parameter is strictly SA and OPF vanish as $1/V$. Remarkably, at zero temperature the value $G = 1/3$ is universal and independent of system size. In Chap. 4 we will see that this is related to the existence of gap-less excitations.

The behaviour of A is different and is schematised in Fig. 3.3. A is a measure of the fluctuations of the spin glass susceptibility $\chi_{\rm SG} = V\overline{\langle q^2 \rangle}$, so that if the ground state is unique it vanishes at $T = 0$ because the overlap is equal to 1. In contrast to G, it only remains finite below T_c provided OPF do not vanish in the thermodynamic limit. In this case A is a non-trivial function of the temperature whose specific shape depends on the particular form of RSB that describes the low-temperature phase, but close to $T = 0$ it always vanishes linearly in T . Actually, we will see in the following chapter that in a finite system of linear size L, A vanishes at low temperatures as $A \sim T\ L^{-\theta}$ where θ is the thermal exponent describing the (free-)energy cost of creating a droplet (see Sec. 2.3). In a RS phase, A vanishes below T_c in the limit $L \to \infty$ so that $\theta > 0$. Nevertheless,

[5] A system is stochastically stable if its physical properties change smoothly when a random perturbation is introduced [FPMP99].

exactly at T_c it may remain finite because any thermodynamical observable in non-self-averaging at the critical point [AH96]. This has been observed in numerical studies of diluted models where the equivalent of A in terms of the magnetisation is found to vanish at every temperature except at T_c [BFMM$^+$98b, BFMM$^+$98a]. Note that we have not said anything about the exact value that G takes at T_c since it might be different from $1/3$.

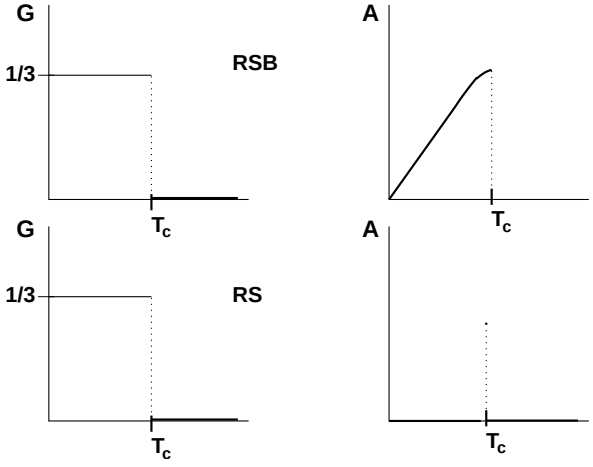

Figure 3.3. Schematic behaviour of G and A in the thermodynamic limit assuming that the conjecture $G = 1/3$ for $T < T_c$ holds. *Top*: when RSB is broken at the transition and *bottom*: when the low-temperature phase is replica symmetric. Note that the shape of A is only a guess but that it could have a different behaviour.

We have to point out that parameters measuring OPF remain always positive even when TRS is absent in the Hamiltonian whereas B can become negative [HK00b]. But in any case, we expect that critical exponents for A, B and G will be the same and coincide with those obtained from the singular part of the free-energy ($\nu_{\rm P} = \nu$ - the usual correlation length exponent). The equivalent of A (3.6) defined in terms of the magnetisation instead of the overlap has been extensively studied by numerical simulations for diluted models [BFMM$^+$98b, BFMM$^+$98a] and for the Ashkin-Teller random bond model [WD95]. In both cases the exponents associated with A and B have been shown to be the same within numerical precision. Here we reach the same conclusion for all the models under analysis.

In the absence of TRS, $\langle q \rangle$ is finite so that we can also study the connected versions of G, A and B defined as follows [PPR99],

$$A_c = \frac{\overline{\langle (q - \langle q \rangle)^2 \rangle^2} - \overline{\langle (q - \langle q \rangle)^2 \rangle}^2}{\overline{\langle (q - \langle q \rangle)^2 \rangle}^2}, \tag{3.10}$$

$$G_c = \frac{\overline{\langle (q-\langle q\rangle)^2\rangle^2} - \overline{\langle (q-\langle q\rangle)^2\rangle}^2}{\overline{\langle (q-\langle q\rangle)^4\rangle} - \overline{\langle (q-\langle q\rangle)^2\rangle}^2} , \tag{3.11}$$

$$B_c = \frac{1}{2}\left(3 - \frac{\overline{\langle (q-\langle q\rangle)^4\rangle}}{\overline{\langle (q-\langle q\rangle)^2\rangle}^2}\right) = 1 - \frac{1}{2}\frac{A_c}{G_c} , \tag{3.12}$$

These parameters vanish as well above T_c and remain finite below the critical temperature when replica symmetry is broken. The behaviour of these quantities with temperature depends on the precise form of RSB describing the frozen phase. But, as well as G, A and B, they also take universal values independent of system size at $T = 0$,

$$\lim_{T\to 0} G_c(V,T) = \frac{13}{31}; \quad \lim_{T\to 0} A_c(V,T) \to \infty; \quad \lim_{T\to 0} B_c(V,T) \to -\infty . \tag{3.13}$$

From the discussion above we can conclude that the study of both quantities G and A is complementary and yields an alternative tool to study the transition and frozen phase of a spin glass: because of its simple behaviour, G is more suitable for locating transitions while only the behaviour of A can tell if OPF remain finite below T_c. The conjecture that $G = 1/3$ below T_c is supported by numerical simulations of mean-field and short-ranged models, suggesting that regardless of the existence of many ergodic components there might be some universal features in the excitations relevant at finite temperatures. Moreover, the study of OPF parameters goes far beyond the models under study in this thesis and has been used successfully in Potts models [HK00b], chiral spin glasses [HK00a] and models for the secondary structure of RNA molecules [PPRT00].

These parameters are useful to study any kind of spin-glass model containing TRS or not. The following sections are devoted to the numerical analysis of mean-field models and the EA model for $d = 1, 2$, and 3. The object is to make a comparative study between OPF parameters and the Binder cumulant to show that already for very small sizes we can get evidence for the transition. The study of mean-field models is important because, as outlined in the introduction, we have a very good theoretical control of many aspects so that we can make many checks of the results obtained from simulations and make a proper comparison with the Binder cumulant. Actually, the behaviour of OPF parameters can be computed in the thermodynamic limit by means of the Replica Equivalence, so that the finite-size corrections to these parameters can be easily evaluated. The analysis is completed with the simulations of the EA model, in which the advantages and drawbacks of OPF parameters are reflexed. On the one hand, these parameters have general properties that offer a general way to characterise the low-temperature phase of these still poorly understood models, even when the sizes studied are small. But, on the other hand, the close link between OPF and the random nature of spin glasses makes these parameters extremely sensible to rare samples. An important difference between the study of OPF parameters and Binder cumulants is that very high precision statistics is needed to compute the first ones. Consider for instance G and G_c. These are ratios of two quantities which may be very small if OPF vanish yielding a large error for G and

G_c. In models where OPF vanish simulating large sizes may then require a prohibitive computational effort. Not only long simulations are needed to thermalise the samples but high-precision statistics is needed to determine with reasonable precision the ratio of two quantities which vanish in the infinite-volume limit. This second limitation is not present in models where OPF are finite such as the SK model or the p-spin model at finite temperature.

2. OPF in mean-field models

2.1 Replica equivalence analysis

In Sec. 2.2 we have seen that the information about the distribution of the order parameter $P(q)$ is contained in the replica matrix Q_{ab}. In the framework of MFT theoretical information about the order parameter is derived using the replica equivalence property (RE) [Par80, BMY84, MPSV84]. Nevertheless, it remains unclear whether in short-ranged systems RE holds in the form presented below. This property states that every row/column of the Q_{ab} matrix is a permutation of any other row/column. Thus, any quantity such as $\sum_b Q_{ab}$ does not depend on a. This is equivalent to impose that the free-energy is extensive in the number of replicas n in order to ensure that there will be no divergences when performing the limit $n \to 0$ [Par98, AC98].

This property imposes some constraints on the $P(q)$, so that one can derive general relations for the probability distributions of several overlaps. The outcome is that any probability distribution function of m overlaps $P(q_{12}, q_{34}, q_{56}, ..., q_{2(m-1)2m})$ can be expressed in terms of the probability distribution of a single overlap $P(q_{12})$ plus all the possible cyclic distributions of $1 < r < m$ overlaps, *i.e.* $P^{12,23,31}$, $P^{12,23,34,41}$, .. $P^{12,23,34,...,m1}$ [Par80, PRT00].

In the computation of any of the OPF parameters, we have to deal with terms involving one or more overlaps which in terms of the replica matrix Q_{ab} read,

$$\overline{\langle q^k \rangle} = \frac{1}{n(n-1)} \sum_{ab} Q_{ab}^k = \int dq P(q_{12}) q_{12}^k \equiv q_k \ , \tag{3.14}$$

$$\begin{aligned} \overline{\langle q \rangle^y} &= \frac{\sum_{a,b,c,d...,l_{2(y-1)},l_{2y-1}} Q_{ab} Q_{cd} .. Q_{l_{2y-1},l_{2y}}}{n(n-1)(n-2)...(n-(2y-1))} \\ &= \int dq_{12} dq_{34} .....dq_{2y\ 2y-1} P(q_{12}, q_{34} ....q_{2y-1\ 2y}) q_{12} q_{34} .....q_{2y\ 2y-1} \ . \end{aligned} \tag{3.15}$$

Here sums run over different indexes. Note that we have defined the q_k's in order to simplify the notation in the forthcoming analysis.

Computation of G

In the computation of G we only need to deal with terms containing one or two overlaps,

$$\overline{\langle q^2\rangle} = \frac{1}{n(n-1)}\sum_{ab} Q_{ab}^2 = \int dq P(q) q^2 \equiv q_2 \ , \tag{3.16}$$

$$\overline{\langle q^4\rangle} = \frac{1}{n(n-1)}\sum_{ab} Q_{ab}^4 = \int dq P(q) q^4 \equiv q_4 \ , \tag{3.17}$$

$$\begin{aligned}\overline{\langle q^2\rangle^2} &= \frac{1}{n(n-1)(n-2)(n-3)}\sum_{a,b,c,d} Q_{ab}^2 Q_{cd}^2 \\ &= \int dq dq_1 P(q,q_1) q^2 q_1^2 \ .\end{aligned} \tag{3.18}$$

The RE property allows to express the probability distribution of two overlaps in terms of the probability distribution of one overlap: $P(q)$. Hence $\overline{\langle q^2\rangle^2}$ can be written in terms of $\overline{\langle q^4\rangle}$, $\overline{\langle q^2\rangle}$ and $\overline{\langle q\rangle}$.
Quantities involving two overlaps such as,

$$\overline{\langle q^k\rangle\langle q^l\rangle} = \frac{1}{n(n-1)(n-2)(n-3)}\sum_{a,b,c,d} Q_{ab}^k Q_{cd}^l \ , \tag{3.19}$$

can be computed as follows: the sum appearing in (3.19) can be re-expressed as:

$$\sum_{a,b,c,d} Q_{ab}^k Q_{cd}^l = \sum_{ab} Q_{ab}^k \sum_{ab} Q_{ab}^l - 2\sum_{ab} Q_{ab}^{k+l} - 4\sum_{a,b,c} Q_{ab}^k Q_{ac}^l \ . \tag{3.20}$$

In order to compute the last term in the l.h.s of the previous identity we use RE,

$$\sum_c Q_{ac} = \frac{1}{n}\sum_{ac} Q_{ac} \ , \tag{3.21}$$

to obtain,

$$\sum_{a,b,c} Q_{ab}^k Q_{ac}^l = \sum_{ab} Q_{ab}^k \sum_c Q_{ac}^l = \sum_{ab} Q_{ab}^k \left(\frac{\sum_{ac} Q_{ac}^l}{n} - Q_{ab}^l \right) \ , \tag{3.22}$$

Substituting this last result into (3.18) we arrive to the following general relation for two-overlap quantities,

$$\begin{aligned}\overline{\langle q^k\rangle\langle q^l\rangle} &= \frac{(n-4)(n-1)}{(n-2)(n-3)} \frac{\sum_{ab} Q_{ab}^k}{n(n-1)} \frac{\sum_{ab} Q_{ab}^l}{n(n-1)} + \frac{2}{(n-2)(n-3)} \frac{\sum_{ab} Q_{ab}^{k+l}}{n(n-1)} \\ &= \frac{(n-4)(n-1)}{(n-2)(n-3)} q_k q_l + \frac{2}{(n-2)(n-3)} q_{k+l} \ .\end{aligned} \tag{3.23}$$

In the particular case of $\overline{\langle q^2\rangle^2}$ we read off $l = k = 2$ in (3.23) to obtain,

$$\overline{\langle q^2\rangle\langle q^2\rangle} = \frac{(n-4)(n-1)}{(n-2)(n-3)} \left(\frac{\sum_{ab} Q_{ab}^2}{n(n-1)} \right)^2 + \frac{2}{(n-2)(n-3)} \frac{\sum_{ab} Q_{ab}^4}{n(n-1)}$$

$$= \frac{(n-4)(n-1)}{(n-2)(n-3)} q_2^2 + \frac{2}{(n-2)(n-3)} q_4 \ . \tag{3.24}$$

Setting n to zero (which means going to the thermodynamic limit) we recover the well known Guerra relations [Gue96] ,

$$\overline{\langle q_{12}^2 \rangle^2} = \frac{1}{3}\overline{\langle q_{12}^4 \rangle} + \frac{2}{3}\overline{\langle q_{12}^2 \rangle}^2 \ . \tag{3.25}$$

that are equivalent to the sum rule (3.14). Now we are ready to compute the the numerator and denominator of G in (3.5),

$$\begin{aligned} \text{numerator} &= \frac{2}{(n-2)(n-3)} \left(\int dq P(q) q^4 - (\int dq P(q) q^2)^2 \right) \\ \text{denominator} &= \int dq P(q) q^4 - \left(\int dq P(q) q^2 \right)^2 \\ &\to \lim_{n\to 0} \ G = \frac{\text{numerator}}{\text{denominator}} = \frac{1}{3} \ , \end{aligned} \tag{3.26}$$

Thus, provided OPF $(\int dq P(q) q^4 - (\int dq P(q) q^2)^2)$ do not vanish below T_c we find that G has a trivial behaviour,

$$G = \frac{1}{3}\Theta(T - T_c) \ . \tag{3.27}$$

As we have already noted, this result can hold even in spin-glass systems with a marginally stable replica symmetric phase. Notwithstanding this, there is no such general simple behaviour for A and B. In the limit $n \to 0$, parameter A reads,

$$A = \frac{q_4 - q_2^2}{3\ q_2^2} \ . \tag{3.28}$$

To compute G_c or any of the other disconnected quantities B_c and A_c, one has to deal with the joint probability of three and four overlaps, so that one has more complicated objects. Therefore, we expect that at finite T the behaviour of connected quantities, as well as for B and A depends on the particular pattern of RSB describing the frozen phase.

For the sake of simplicity calculations leading to the final expressions for connected quantities are reported in Appendix A. In the high-temperature phase all these parameters vanish in the infinite-volume limit. In what follows the behaviour of these quantities below T_c in the simplest patterns of RSB are discussed.

2.1.1 The symmetric case

In the symmetric case all the off-diagonal terms in the replica matrix are equal $Q_{ab} = q \neq 0$, thus OPF are strictly zero. Therefore, A vanishes except at the transition point where it takes a finite universal value. The Binder cumulant is equal to 1 in the frozen

phase, except at the transition point where it also takes a finite universal value. In connected quantities, as well as in G, both numerator and denominator vanish, thus we cannot use results derived through RE to obtain information about how these parameters behave below T_c. All the same, numerical results for the spherical SK model (see Sec. 2.4) and for the EA model in 3d (Sec. 3.3) [PRS02] support the conjecture that G takes the value $1/3$ in the SG phase.

2.1.2 One-step replica symmetry breaking

As explained in Sec. 2.2.1 this is the simplest version of breaking replica symmetry in the Parisi scheme. The elements of the Q_{ab} matrix are distributed in boxes of size m and can take two different values: q_1 for the elements inside the blocks along the diagonal and q_0 otherwise. With this particular pattern we obtain the following expressions for A and B (for details of the calculations see Appendix A),

$$A = -\frac{(m-1)\,m\,(q_1^2-q_0^2)^2}{3((m-1)\,q_1^2-m\,q_0^2)^2}\,, \tag{3.29}$$

$$B = \frac{(m-1)\,q_1^4-m\,q_0^4+3((m-1)\,q_1^2-m\,q_0^2)^2}{2((m-1)\,q_1^2-m\,q_0^2)^2}\,. \tag{3.30}$$

Therefore, these parameters depend on the specific values of q_1, q_0 and m for a particular model. Notwithstanding this, connected quantities only depend on the size of the blocks, m, that in general is a function of temperature (see Appendix A):

$$G_c = \frac{39-113m+98m^2}{93-221m+266m^2}\,, \tag{3.31}$$

$$A_c = \frac{39-113m+98m^2}{140m(1-m)}\,, \tag{3.32}$$

$$B_c = \frac{-3(31-167m+182m^2)}{280m(1-m)}\,. \tag{3.33}$$

The simple functional dependence on m of A_c, G_c and B_c allows us to establish several universal features of these parameters (see Fig. 3.4). In first place, we note that below T_c, because $m \in [0,1]$, G_c always remains finite and positive. At $T=0$, since $m=0$ in any system, it takes the universal value $13/31$. In the same way, at $m=1$, G_c takes another universal value: $G_c = \frac{14003-2520\sqrt{11}}{50111} \approx 0.174$. Another interesting feature of G_c is the existence of a local minimum at $m^* = \frac{3}{20}(1-\sqrt{11}) \approx 0.650$ whose value $G_c = 4/23$ is universal for all the systems exhibiting one-step RSB. As we will show in a forthcoming section, this is important from the point of view of numerical results for small sizes as the asymptotic position of this minimum can give us information about the behaviour in the thermodynamic limit and thus about the dependence of m on T.

In second place, we note that both A_c and B_c diverge at $m=0$, and therefore at zero temperature, the same being also true at $m=1$. The difference between both is that

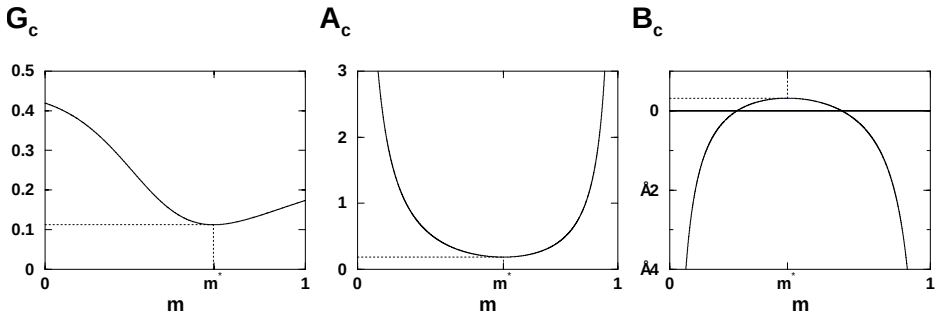

Figure 3.4. Connected quantities in the one-step RSB ansatz. G_c, A_c and B_c versus m in the range $[0,1]$ after the expressions (3.31),(3.32) and (3.31). The m^*'s signal the local extreme of each parameter as commented in the text.

while A_c remains *always* positive and has a minimum at $m^* = (13 - 2\sqrt{26})/5 \approx 0.560$ (whose universal value is $A_c = -1/4 + 3\sqrt{26}/35 \approx 0.187$), B_c diverges to $-\infty$ and displays a maximum at a positive value $B_c = (315 - 6\sqrt{1426})/280 \approx 0.316, (m^* = (-31\sqrt{1426})/15 \approx 0.451)$.

Unfortunately, for the two-step RSB scheme (and further RSB), we do not have such a simple expression and numerical computations for each particular model have to be performed. In the following sections we analyse three mean-field models for which the analytical solution is known: the SK model with and without a field, the p-spin $(p = 3)$ Ising model and the SK spherical spin glass. The two former ones are known to exhibit RSB of different kinds: a full-step and a one-step RSB respectively, whereas the latter has a a replica symmetric phase. Therefore, these systems can provide a direct check of the results reported in this section.

Note that the conjecture for G as well as all the previous results are valid for Ising spins and not for continuous-spin models in general. In a forthcoming section we shall study the spherical SK model. Despite spins are continuous, we expect the conjecture to hold because in the frozen phase the distribution of the modulus of each spin variable is very peaked around 1.

2.2 The Sherrington-Kirkpatrick model

The Sherrington-Kirkpatrick model one of the most celebrated spin-glass models and has been exhaustively studied both theoretically as outlined in the introduction (Sec. 2.2) and numerically (for very precise simulations see [CMPR00, MZ00]).

Here we intend to discuss the numerical results obtained for the OPF parameters defined in the previous section and make a comparison with the Binder parameter. We consider the SK model in a field defined by (1.24),

$$\mathcal{H} = -\sum_{i<j} J_{ij}\ S_i\ S_j\ -\ h\sum_i S_i\ , \qquad S_i = \pm 1 \tag{3.34}$$

where h is the magnetic field acting on V spins, and the couplings are random variables with variance $\frac{1}{V}$ in order to preserve the extensivity of the energy.

This model has a transition in which RS is broken at infinite step at a critical temperature $T_c(h)$ given by the AT instability line (2.5). Therefore we expect the curves for different parameters to cross at this point. The behaviour close to T_c has been studied analytically in the case of no applied field. The free-energy can be expanded is terms of the Q_{ab} matrix for small values of q to find that the finite volume correction to the thermodynamic limit behaviour scales as $\sim (T - T_c)\ V^{\frac{1}{3}}$ [PRS93a, PRS93b]. As a matter of fact, as in any mean-field model the correlation length exponent is $\nu = 1/2$. Since the upper critical dimension is $ucd = 6$ we read off $\nu d = 3$ and thus we expect that B, G and A are a function of $(T - T_c)^3\ V$.

2.2.1 Numerical results

The analysis of OPF parameters in this model with and without a field had already been done in [HK00b] and [MNP$^+$98a] respectively, but the fact that already from very small system sizes the transition can be determined had not been exploited. In the case of zero field only connected quantities can be studied because TRS is contained in the Hamiltonian. But, in the case of applied field the whole family of parameters can be studied. We have studied OPF parameters in three different cases $h = 0,\ 0.3$ and 0.6. The transition temperatures obtained from evaluating numerically the AT line (see Fig. 2.1) are $T_c(0) = 1, T_c(0.3) = 0.65$ and $T_c(0.6) = 0.48$.

Parameters of the simulations: The study for very small sizes $V = 4, \cdots, 11$ has been done through the exact computation of the partition function of 100000 samples of Gaussian quenched couplings with variance $\frac{1}{V}$, following the analysis for the $h = 0$ case made in [Yp82]. Larger systems have been studied using in the case in a field, simple Monte Carlo simulations with around 1000 samples of Gaussian distributed couplings for sizes $V = 13,\ 17,\ 23,\ 33$ and the parallel tempering technique [HN96, HTY98] with a number of samples ranging from 1000 for the smallest size to 250 for the biggest one. We have also studied larger system sizes $V = 32, 64, 128, 256, 512$ with a Binary distribution of the couplings (1.14) using Monte Carlo dynamics. The differences between the results obtained with Binary and Gaussian couplings are expected to vanish very fast with system size, and indeed we have checked that for $V = 32$ and Binary coupling the results are nearly the same as the ones obtained with Gaussian couplings for $V = 33$.

- SK with no field

  In Fig. 3.5 we plot A and G versus temperature for small and large sizes in the top and bottom panels respectively. Fig. 3.6 shows the Binder ratio B for both groups of sizes and in Fig. 3.7 show the scaling plots for B (a) and G (b) for the larger sizes.

  As this system contains TRS, the Binder cumulant for different sizes is expected to exhibit a crossing of the curves for different sizes [BY88, HK00b]. Indeed, this is what we observe for the large sizes. However we must note that, while even for very small samples we do observe a crossing for G and A at T close to $T_c = 1$ (Fig. 3.5), for the same sizes, curves for B do not display such a crossing (Fig. 3.6 (a)). In

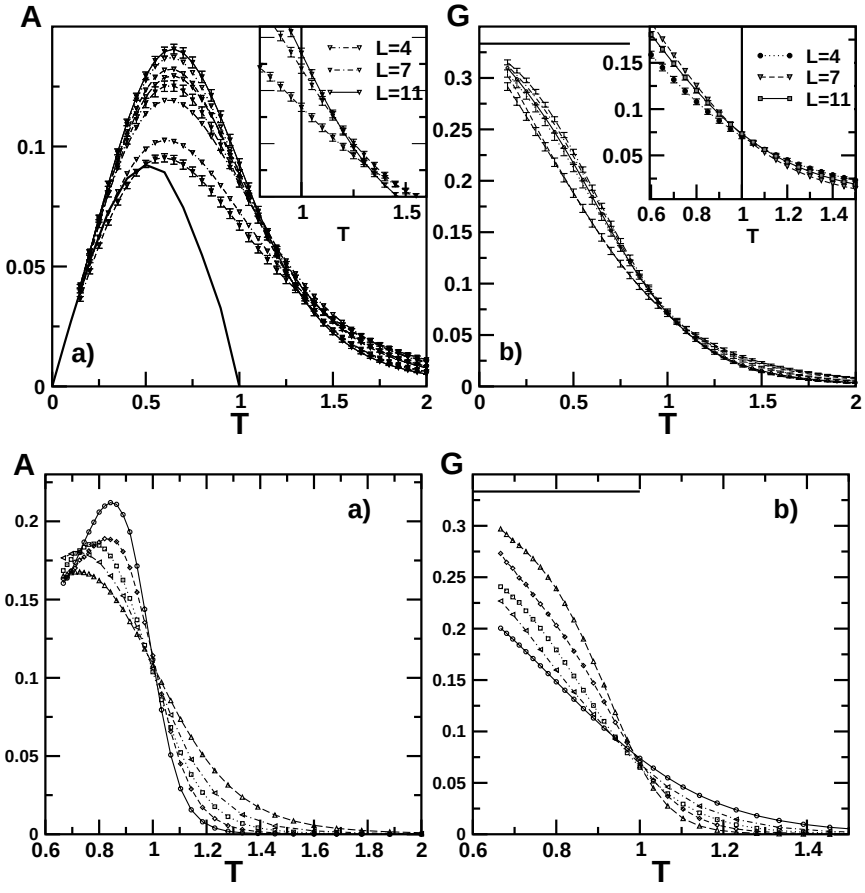

Figure 3.5. Parameters A (plot a) and G (plot b) for the SK model with no external field. *Top:* Results for small sizes $V = 4, \cdots, 11$ from bottom to top at low T. Error bars are shown for sizes $V = 4, 7, 11$. In both insets we show in detail the crossing region for these sizes. The solid line in (a) corresponds to numerical results of the one-step approximation (3.29), obtained from solving numerically the saddle-point equations of the SK model for this particular case [MPV87, FH91a]. *Bottom:* Results for large sizes $V = 32, 64, 128, 512$ from bottom to top in the high T region.

Fig. 3.6 we have plotted the Binder ratio for $V = 32$ together with the smaller sizes to stress that we have to increase the size of the system (*i.e.* reach $V \approx 100$) to observe the crossing and not only a merging of all the curves in the low T region. We have to remark that the crossing point for OPF parameters approaches T_c from high temperature but in the Binder cumulant T_c is approached from low temperatures.

The finite-size scaling analysis shown in Fig. 3.7 shows that OPF parameters verify the FSS ansatz with the same exponents and critical temperature as the Binder cumulant. The scaling variable is that of the free-energy and magnetisation: $V\,(T -$

$T_c)^3$ [PRS93a, PRS93b]. The collapse of the data, which are shown only for $T - T_c > 0$, is very good, not only for B but also for G (the same being true for the parameter A).

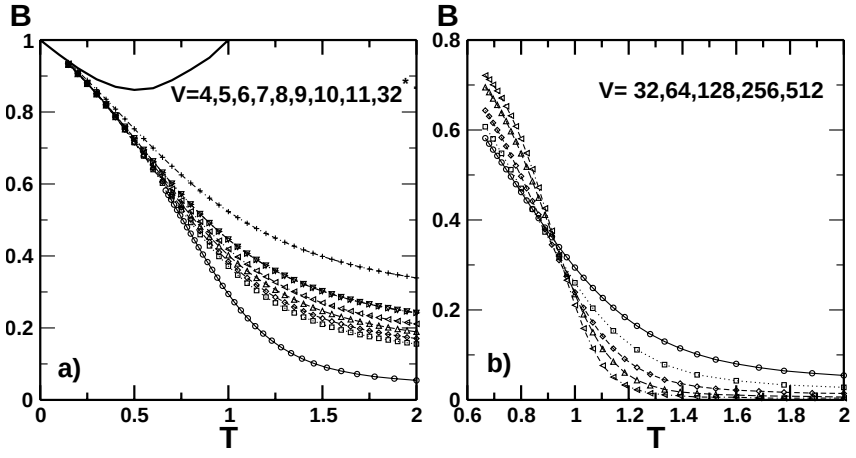

Figure 3.6. Binder ratio, B, for the SK model with $h = 0$: (a) for small systems ($V = 4, 5, 6, 7, 8, 9, 10, 11$ from top to bottom) and (b) for $V = 32, 64, 128, 512$ from top to bottom at high T.

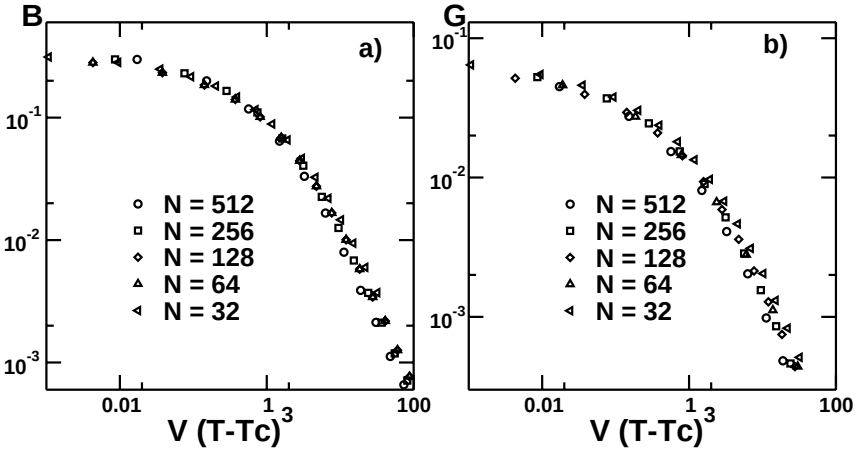

Figure 3.7. Scaling functions: B (a) and G (b) for the SK model with $h = 0$ versus the scaling variable $V\,(T - T_c = 1)^3$ for sizes $V = 32, 64, 128, 512$.

- Finite-field simulations

On analysing the low-temperature behaviour of OPF parameters it turns out that there are two conditions which have to be fulfilled in order to recover the universal values

at zero temperature: the uniqueness of the ground state and the absence of gap in the local-field distribution (see Chap. 4). This last requirement is assured in small systems by our choice of Gaussian couplings. However in order to study connected quantities there is also another requirement the system must not present TRS. In general, this is the situation in systems with applied field. Despite, it turns out that in small systems with an even number of spins there can be rare samples whose ground state has zero magnetisation and thus is twofold degenerate. This implies that the low-temperature behaviour of connected quantities yields different values from the expected universal ones such as $G_c = \frac{13}{31}$ (see the inset in the plot for G_c in Fig. 3.8 where G_c becomes greater than $13/31$ and goes to 1 at $T = 0$). This situation does not take place when there is an odd number of spins, thus only odd samples can be studied in order to obtain sensible results.

In Fig. 3.8, we plot G, G_c and A at field $h = 0.3$. Results for G_c and G for the largest field, $h = 0.6$ are shown in Fig. 3.10. In Figs. 3.9 and 3.11 we show A_c, the Binder ratio and its corresponding connected quantity for both applied fields, $h = 0.3$ (a) and $h = 0.6$ (b).

- Small fields: $h = 0.3$.
  In Fig.s 3.8 and 3.9 results for the lowest field are shown. It is remarkable that G, G_c, A and A_c display a clear crossing of the curves which is not seen neither for the Binder ratio where curves for all sizes seem to merge at low temperatures (Fig. 3.11 (a)), nor for B_c (Fig. 3.11(b)). Nevertheless, there is a clear difference between disconnected parameters (G and A) and connected ones (G_c and A_c). The crossing for disconnected quantities, A and G, takes place at a temperature which is higher than 1 for small samples and slowly approaches 1 as we increase the size. On the contrary, results for A_c and G_c, display a crossing at a temperature which already for small samples is smaller than one and approaches the predicted $T_c(0.3) = 0.65$ as we increase the size of the system. Indeed, for the largest sizes $V = 29, 33, 64$ curves cross around $T = 0.65$ (Fig. 3.8 (c)).
- Large fields: $h = 0.6$.
  For large fields the transition temperature is very low so that thermalisation problems make it difficult to get accurate numerical results. In spite of this, results for G, G_c and A_c displayed in Figs. 3.10 and 3.9 (b) show a great difference between G and G_c. While the crossing for G takes place at very high temperatures (close to 2) , curves for G_c cross at a temperature that already for small samples is not very far from the theoretical value $T_c = 0.48$ and gets closer to it as we increase the size. From the Binder cumulant (Fig. 3.11 (b)) one gets no clear information. Numerical results display a crossing at high temperature as curves for G do, but the crossing point seems to be moving toward higher temperatures with system size suggesting that this crossing has no real connection with the existence of a transition. Still, curves for B_c (Fig. 3.11 (b)) show an interesting result, since we observe a crossing around $T = 0.5$. Unfortunately, results are not very clean

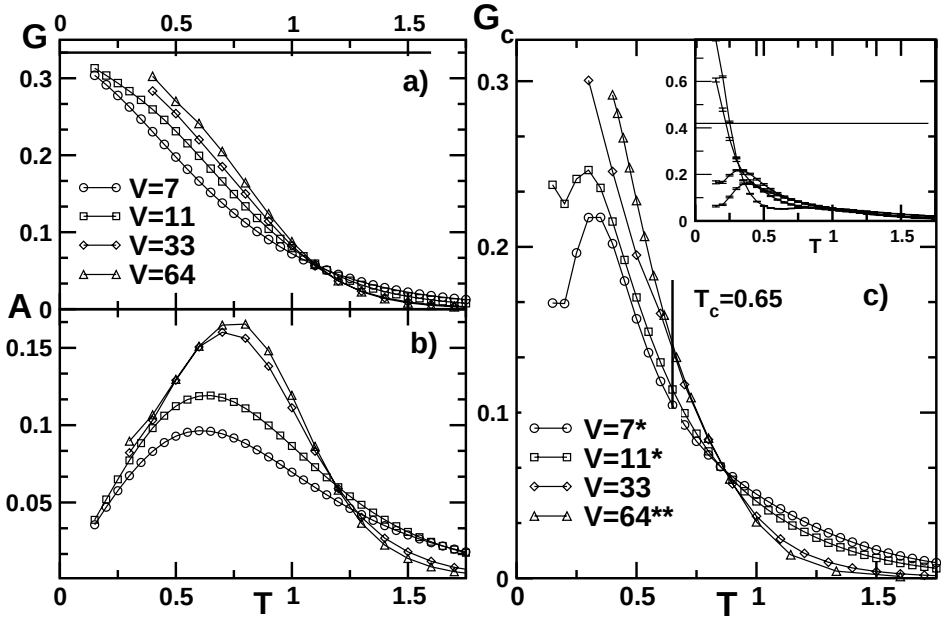

Figure 3.8. Results for the SK model in a field $h = 0.3$ for system sizes $V = 7, 11, 33, 64$ from top to bottom in the high temperature region. a) Parameter G the full line corresponds to the infinite-volume limit result $G = 1/3$. b) Parameter A c) Parameter G_c. Note that in there's no full line standing for the $T = 0$ value of G_c as it falls out of scale. The solid vertical line indicates the transition temperature $T_c = 0.65$. In the inset at the top right corner, we show the low T behaviour of G_c for small samples with an even number of spins $V = 6, 8$ from top to bottom, the full line corresponds to the $T = 0$ value $G_c = 13/31$. Curves below the line correspond to samples with odd number of spins $V = 3, 5$.

because the transition takes place at a very low temperature and thermalisation is not easy. For this reason the crossing of curves for A_c in Fig. 3.9 (b) is blurred by the existence of the divergence at $T = 0$. Notwithstanding this, these results, together with the results in [PR94] for the $P(q)$, which for very large sizes presented two peaks in the positions predicted by the RSB solution, are the most clear evidence for a transition in such a high field ($h = 0.6$) which has been reported up to now.

2.3 The p-spin Ising model; $p = 3$.

In Sec. 1.1 we have already introduced the p-spin models that for $p > 2$ display a one-step RSB transition with a discontinuity in the order parameter which has many points in common with the glass transition in structural glasses [pT87, pW87, Méz00]. It is particularly interesting that a measure of the violation of FDT in glasses can give us information on the pattern of RSB, *i.e.* on the parameter m which determines the

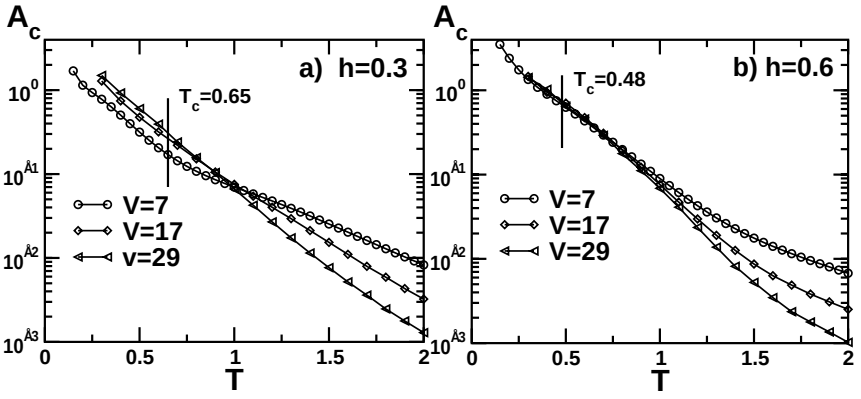

Figure 3.9. A_c for the SK model in applied field for sizes $V = 7, 11, 13, 23, 29$: (a) for $h = 0.3$, (b) for $h = 0.6$. The solid vertical line indicates the corresponding transition temperature.

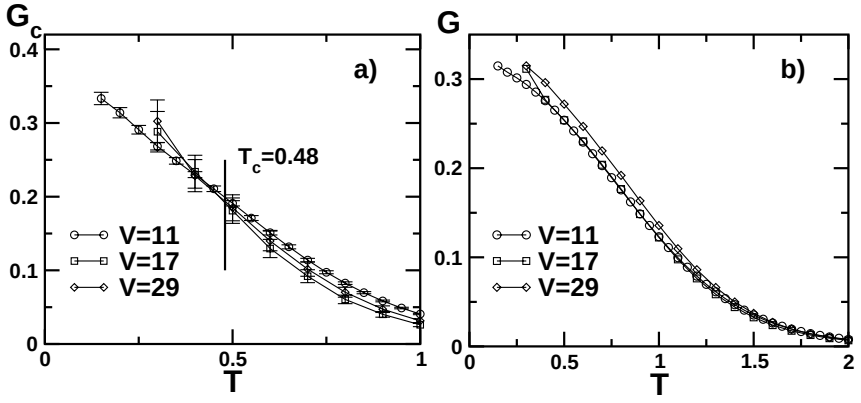

Figure 3.10. G_c (a) and G (b) for the SK model in a field $h = 0.6$ for sizes $V = 11, 17, 29$. The solid vertical line indicates the transition temperature.

structure of the replica matrix Q_{ab} and which we have already shown in Sec. 2.1 that controls the behaviour of connected quantities.

We have chosen to study the $p = 3$ case because it does not contain TRS in the Hamiltonian and therefore admits a study of the whole family of parameters. The model is defined by the following Hamiltonian,

$$\mathcal{H} = -\sum_{i_1,i_2,i_3} J_{i_1,i_2,i_3} S_{i_1} S_{i_2} S_{i_3}\,; \qquad S_i = \pm 1 \quad , \tag{3.35}$$

where couplings are Gaussian variables with zero mean and variance $\frac{3!}{2V^3}$. The transition temperature is given by (2.7), yielding $T_c \approx 0.65$ [Der81, Gar85].

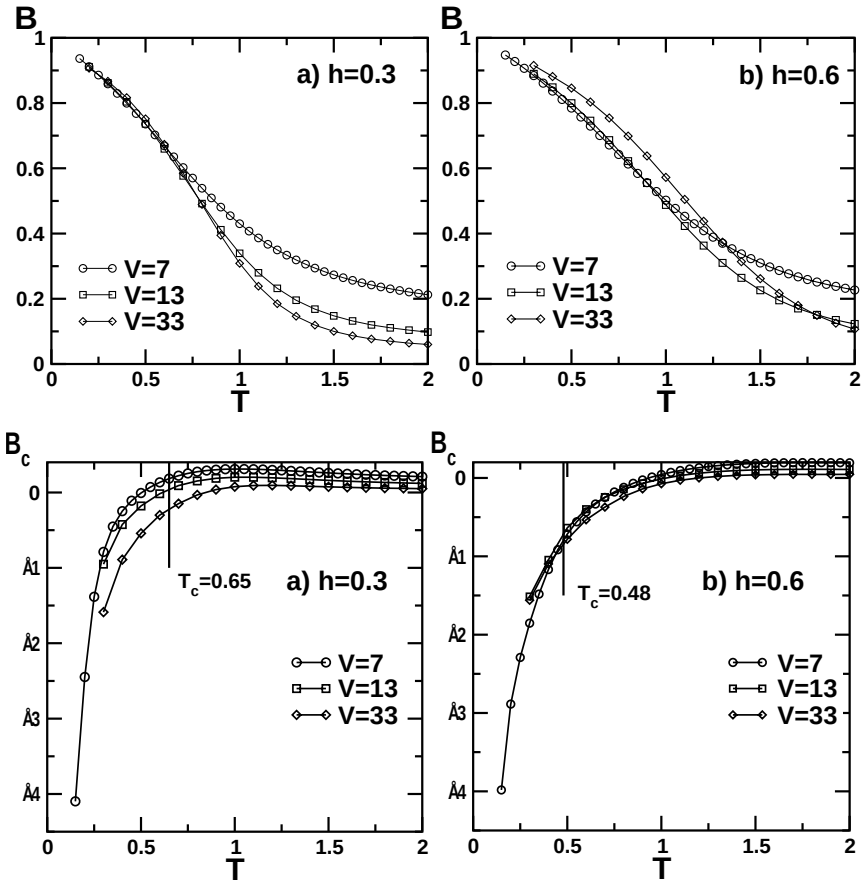

Figure 3.11. Binder Cumulant (*top panels*) and its corresponding connected version B_c for the SK model with an applied field (a) $h = 0.3$ and (b) $h = 0.6$ for sizes $V = 7, 13, 33$. The solid vertical line indicates the transition temperature in each case.

The outcome of numerical simulations can provide us with a direct check of the validity of identities (3.31), (3.32) and (3.33) for the finite-T behaviour of G_c, A_c and B_c respectively [6]. Moreover, this model presents a further simplification since q_0, the off-diagonal block value of the replica matrix element Q_{ab}, vanishes below the transition. For this reason, expressions for A and B in (3.29) and (3.30) have a much simpler expression only in terms of m :

$$A = \frac{m}{3\,(1-m)}\,, \qquad B = \frac{2-3\,m}{2\,(1-m)}\,. \tag{3.36}$$

[6]Note that in Sec. 1.1 we have said that at lower temperatures these models display a transition into a full-step RSB phase. Thus the one-step solution is not exact, but is a very good approximation because the breaking is very small [Gar85].

2.3.1 Numerical results

Parameters of the simulations: We have made exact numerical computations of the partition function for sizes ranging from $V = 4$ up to 11 averaging over 10000 samples and Monte Carlo simulations using the parallel tempering technique for $V = 13, 17, 23, 29, 33$ averaging over $150-500$ samples.

In Figs. 3.12 and 3.13 we plot B, G_c, G, A, A_c and B_c versus temperature. The full line corresponds in each case to the theoretical prediction obtained by numerically solving the saddle-point equations.

The results for the Binder parameter (Fig. 3.12) do not display any crossing but show that around the transition temperature, $T_c = 0.65$, B becomes negative, and has a minimum which grows with the size of the system. This in agreement with the infinite-volume expression (3.36) which indicates that at the transition, where $m = 1$, the Binder ratio has a negative divergence. Nevertheless, this is not a general feature of one-step RSB transitions since B strongly depends on the actual values of q_1, q_0 and m, *e.g.* in the Potts model (see Fig. 3.2) B is is expected to be -1 at the transition (see Fig. 3.2) [HK00b]. Results for B_c are very similar, since there is no crossing, and there is also a minimum around T_c which deepens with size. The absence of crossing is due to the fact that curves for different sizes approach to the infinite-volume behaviour from top to bottom as we can see in Figs. 3.12 (b) and 3.13 (b) respectively.

Instead, our results for G_c, G, A and A_c exhibit a crossing which moves from higher to lower temperatures giving evidence for the existence of the transition. As we have noted in the previous section, we observe that finite-size corrections to T_c are bigger in disconnected averages than in connected ones, the formers giving a better estimate of the transition temperature. However, it is important to point out that the position of the maximum of A which accounts for the existence of a phase where replica symmetry is broken has a quick saturation towards $T = 0.6$, and grows with size as is expected from the divergence that this parameter shows at the transition (3.36). A similar situation is met in results for A_c (Fig. 3.13), since there is also a predicted divergence at $m = 1$, which is numerically observable by a maximum around T_c which grows and sharpens with size.

From the results for G_c, we can still go a bit further. We observe that, as the size increases, the shape of the curve approaches the one of the thermodynamic limit much faster than in the other parameters, due to the softer behaviour of G_c. It is interesting to note that even though we see a crossing of the curves which moves toward T_c from higher temperature as V increases, clearer evidence for the existence of the transition and the kind of transition (*i.e.* one-step RSB) comes from the existence of a bump which becomes closer to T_c as the size grows. At low temperatures, curves always remain under the infinite-volume line, so that there is no crossing in the low T phase. Note that curves quickly stuck to the minimum displayed by the infinite-volume line for G_c.

The results for the SK model show that connected quantities exhibit quite a different behaviour, as the curves are smooth and do not show any concavity, nor divergence at the transition temperature. Hence, from the behaviour of G_c, A_c, B_c, A and B, we can infer

the type of RSB that takes place at the transition, extending the previous comparative analysis made in [HK00b] between the 3-Potts model and the SK with no field.

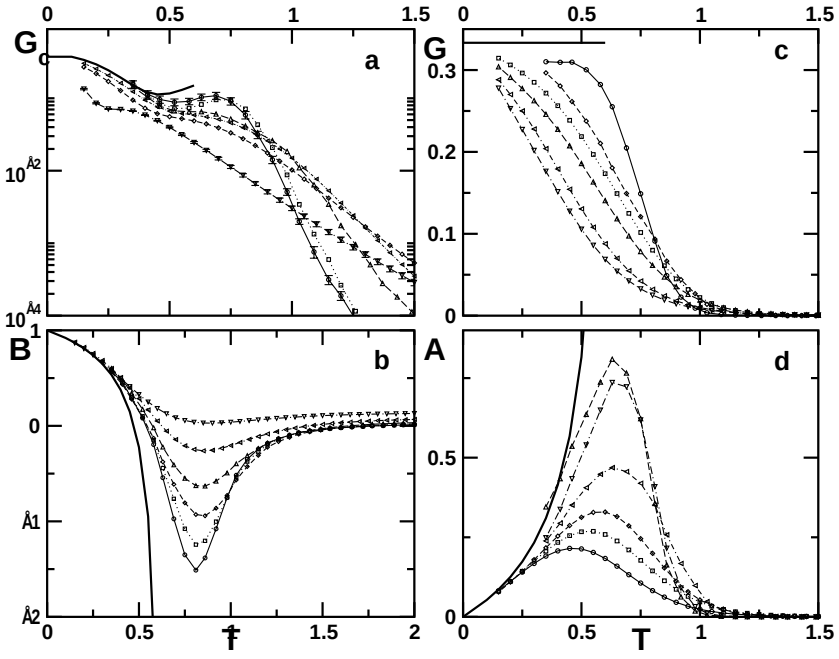

Figure 3.12. We show the results for the 3-spin model for sizes ranging from $V = 4$ to $V = 33$. In every plot, the solid line corresponds to the theoretical prediction of expressions (3.27), (3.31), (3.36) for G, G_c and A and B (see text): (a) G_c for sizes $V = 4, 7, 11, 17, 29, 33$ from top to bottom in the low T region; errors bars are displayed for the larger and smaller sizes. (b) B (Binder ratio) for sizes $V = 7, 11, 17, 23, 29, 33$ from bottom to top. (c) G for sizes $V = 4, 8, 11, 17, 29$ from bottom to top in the low-temperature region. (d) A for sizes $V = 5, 8, 11, 17, 29, 33$ from bottom to top in the low-temperature region.

2.4 The Sherrington-Kirkpatrick spherical model

This model is an example of a spin glass with a replica symmetric phase in which OPF strictly vanish in the thermodynamic limit. Since parameter A vanishes the object is to analyse the behaviour of parameter G at finite temperature compared to that of the Binder cumulant.

As described in Sec. 2.8 the spherical SK model consists of continuous spins that satisfy a global spherical constraint whose Hamiltonian reads (2.8),

$$\mathcal{H} = -\sum_{i<j} J_{ij}\sigma_i\sigma_j\,; \qquad \sum_{i}^{V}\sigma_i^2 = V\,; \qquad -\infty < \sigma_i < \infty\,. \tag{3.37}$$

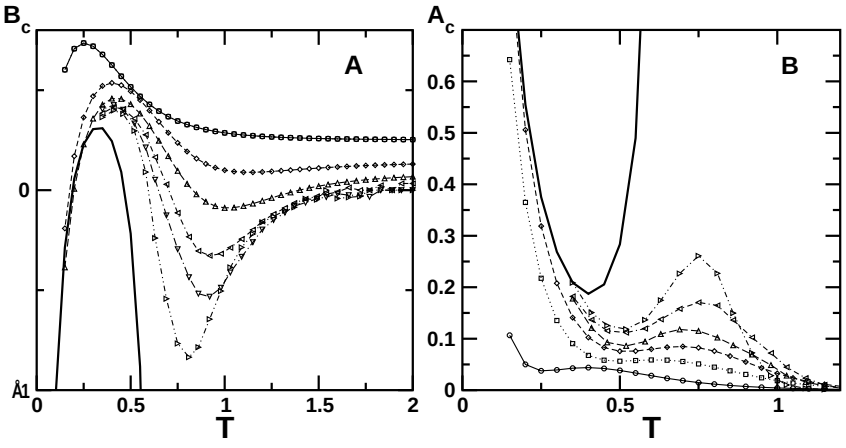

Figure 3.13. Results for the 3-spin model: (a) B_c for sizes $V = 4, 7, 11, 17, 23, 29$ from top to bottom, and (b) A_c for sizes $V = 4, 7, 11, 17, 23, 29$ from bottom to top (in the low T region). The solid line corresponds to the numerical evaluation of expressions (3.32) and (3.33) for A_c and B_c respectively.

Couplings are Gaussian distributed variables with zero mean and variance $1/V$.

AT $T_c = 1$ this model has a transition into a RS phase with $q = 1 - T$. This solution is the only possible one in the Parisi scheme, however it is only marginally stable against an Ising type perturbation [JR89]. Actually, when computing the eigenvalues of the Hessian Matrix it turns out that the *replicon* eigenvalue is zero at every temperature below T_c. This situation is analogous to that of the SK model and implies that the susceptibility diverges in the low-temperature phase. However, because the phase is RS the susceptibility diverges $\sim V^{1-\alpha}$ with $\alpha < 1$. This is very relevant when studying the behaviour of parameter G below T_c. As numerator and denominator vanish in (3.5) we have to evaluate finite-size corrections to these quantities to obtain the behaviour of G below the transition. In the SK model, close to T_c finite-size corrections can be evaluated to find that the leading term is $\sim V^{-2/3}$ so that we read off $\alpha = \frac{2}{3}$ [PRS93a]. This is exactly the same exponent that that we find numerically in this model. Despite, in the spherical case, this marginality implies that the susceptibility diverges as $\sim V^{1-\alpha=1/3}$ in contrast to that of the SK model where OPF are finite and χ_{SG} diverges $\sim V$ below the transition.

To compute G we need to know the precise value of the amplitudes entering in the finite-size corrections in the parameters $\overline{\langle q^2 \rangle}$, $\overline{\langle q^2 \rangle^2}$, $\overline{\langle q^4 \rangle}$. However, as analytical calculations of finite-size corrections in spin glasses are extremely difficult here we will take numerical and theoretical considerations relying on results obtained for the SK model [PRS93a, PRS93b].

2.4.1 Numerical results

We have numerically evaluated the following quantities entering in the computation of G and B $\overline{\langle q^2 \rangle}^2$, $\overline{\langle q^2 \rangle^2}$, $\overline{\langle q^4 \rangle}$ for different temperatures and sizes using the Monte Carlo Method. The data correspond to small sizes, since the interest here is to show that G is a powerful tool to investigate phase transitions since finite-size corrections to T_c are much smaller than in the Binder cumulant.

Parameters of the simulations: the model has been simulated using Monte Carlo dynamics where a spin at random is chosen and the following change is proposed $\sigma_i \to \sigma_i + \delta r_i$ where δ is typically of order 1 and r_i is a random number uniformly distributed between $-1/2$ and $1/2$. The value of δ is chosen such that the acceptance rate is reasonable. The value of all other spins is recalculated in order to satisfy the global spherical constraint. Moves are accepted according to the Glauber algorithm.

The number of samples used is of several thousands for very small sizes ($V = 4, 6, 8, 12, 16$) and several hundreds for larger ones ($V = 24, 32, 40, 48, 64$). The overlaps have been computed by collecting statistics over a large time window (approximately 10^5 Monte Carlo steps for each sample).

Fig. 3.14 shows the results for G and B in the left and right panels respectively. Note that G already for the smallest sizes there is a crossing of the different curves. The crossing appears for values of T well above $T_c = 1$ for the smallest sizes and moves to lower temperatures as the size increases converging to the expected value $T_c = 1$. In contrast, in B the crossing point moves from low temperature to $T_c = 1$ much slowly than the crossing point of G does. Even for the largest sizes the crossing is still at $T \simeq 0.8$ quite far from $T = 1$. This is exactly the same effect found in the p-spin and the SK model reported in the previous sections and found in the literature in other models [BY88, HK00b].

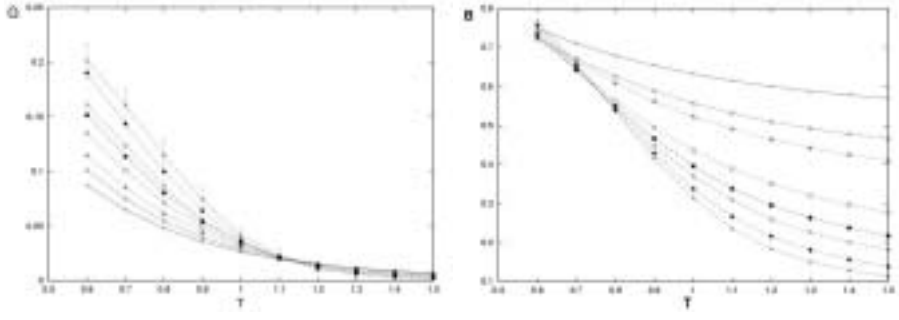

Figure 3.14. Results for G (*left*) and B (*right*) for the SK spherical spin glass ($V = 4, 6, 8, 16, 24, 32, 48, 64$ from below to above at low temperatures). The largest error bars for G are shown for the largest size $V = 64$, for B error bars are negligible.

Another issue which is worth addressing is the behaviour of G in the thermodynamic limit. We recall that it is a conjecture that G is $1/3$ in the thermodynamic limit at all

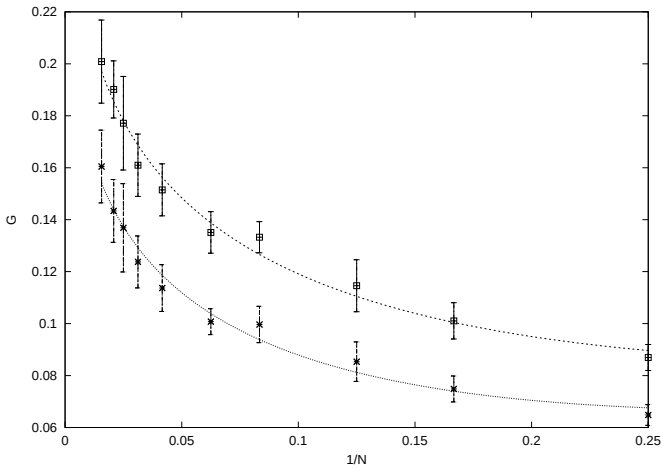

Figure 3.15. Fit function (3.39) to the G parameter for different sizes at $T = 0.6$ (above) and $T = 0.7$ (below). Extrapolations to $V \to \infty$ are compatible with $G(V \to \infty) = 1/3$ in the spin-glass phase.

temperatures below T_c even when OPF vanish as $V^{-\alpha}$ with $0 < \alpha < 1$. Thus the object is to study the finite-size corrections in $\overline{\langle q^2 \rangle}, \overline{\langle q^2 \rangle^2}, \overline{\langle q^4 \rangle}$ to extrapolate the behaviour of G in the limit $V \to \infty$. In this model $\alpha = 2/3$ therefore we expect that finite-size corrections can be expanded in terms of $V^{-2/3}$ so that,

$$\overline{\langle q^2 \rangle}^2, \overline{\langle q^2 \rangle^2}, \overline{\langle q^4 \rangle} = q_{EA}^4 + \frac{a}{V^{2/3}} + \frac{b}{V} + \frac{c}{V^{4/3}} + \frac{d}{V^{5/3}} \quad , \tag{3.38}$$

with $q_{EA} = 1 - T$. From these expressions we expect for G the following behaviour,

$$G = G_\infty + \frac{A}{V^{1/3}} + \frac{B}{V^{2/3}} + O(1/V) \quad . \tag{3.39}$$

We have fitted the values of G to this expression with G_∞, A, B as fitting parameters. The results and the fits are shown in Fig. 3.15. The extrapolated values for the lowest temperatures $T = 0.6, 0.7$ are $G_\infty(T = 0.6) = 0.34 \pm 0.2$, $(A(T = 0.6) = -0.71 \pm 0.1$ and $B(T = 0.6) = 0.49 \pm 0.13)$, $G_\infty(T = 0.7) = 0.29 \pm 0.2$, $(A(T = 0.7) = -0.66 \pm 0.1$ and $B(T = 0.7) = 0..49 \pm 0.12)$. Within errors these are compatible with the value $1/3$. Trying to have an estimate of G_∞ at higher temperatures is very difficult because critical effects are strong. Notwithstanding this, we conclude that for this model the value $1/3$ is well compatible with the data supporting the conjecture that $G = 1/3$, $T < T_c$ is a generic result for any spin glass.

2.5 Summary of the results for mean-field models

Lets us summarise the main conclusions that we can draw from the study of mean-field models.

1 Systems with TRS: A and G are good parameters to locate the transition. Finite-size effects are evidenced by a crossing at a temperature slightly above T_c, that moves towards T_c as size increases. The location of the transition point is more precisely located by G and A than by the Binder ratio, B. Finite-size scaling analysis reveals that B, G and A have the same scaling exponents, thus suggesting that the scaling behaviour of A and G for generic short-ranged systems may be obtained from the standard renormalisation group approach.

2 Systems with no TRS: In general connected quantities, G_c, A_c and B_c show a crossing which gives evidence for a transition. Finite-size corrections to T_c are of the same sign as those in the case $h = 0$.

3 Corrections to T_c: Our observations corroborate previous results [BCF$^+$00] which argued that finite-size corrections to T_c for parameters measuring OPF were of opposite sign than for the Binder parameter. For OPF parameters the crossing point at T^* starts well above T_c and approaches T_c as we increase the size of the system. For the biggest sizes T^* is very close to T_c. On the contrary, curves for B (or B_c) cross at $T^* < T_c$, and therefore, since thermalisation is more difficult at low T, the crossing is harder to observe. Moreover, the crossing for the biggest sizes takes place at a temperature slightly below T_c, thus making it evident that finite-size corrections to T_c are much stronger in the Binder ratio than in A and G.

4 Nature of the transition and behaviour of G: We have seen that, in general, the behaviour of different parameters at T_c and in the frozen phase depends strongly on the type of RSB that takes place at the transition. Notably, in systems with a one-step RSB transition the Binder cumulant can be negative, something that does not happen in systems with full RSB as the SK. Which is the kind of RSB that takes place at the transition cannot be extracted, a priori, from the plots. However, it is remarkable that the general temperature behaviour of the different quantities, A, B, is the same in the SK with and without a field and very different from that of the $p-$spin. This corroborates the results of the previous section: systems exhibiting the same kind of RSB below the transition display qualitatively the same behaviour for A, B, G_c, A_c and B_c.

   Remarkably, the behaviour of G is much more robust to these variations as expected from the RE analysis. The simulations of the spherical model are well compatible with the conjecture that the behaviour of G is universal in the whole low T phase.

3. OPF in short-ranged systems: the Edwards-Anderson model

Here we are interested in studying what information can be obtained about the frozen phase of this model from the behaviour of OPF parameters, G and A. The model consists of Ising spins sitting on a cubic lattice of dimension d interacting with nearest (nn) or

next nearest neighbours (nnn),

$$\mathcal{H} = -\sum_{\langle i,j \rangle} J_{ij} S_i S_j \quad . \tag{3.40}$$

In our numerical analysis the couplings are Gaussian variables with variance 1. We have considered the nn case for $d = 1, 2$ and the nnn case in $d = 3$. We have already noted that OPF parameters are very demanding at a computational level because very high precision statistics are needed. Because thermalisation problems are so large the number of samples is rather modest, so that in these cases with TRS, G and A work worst than other parameters such as the Binder cumulant or the correlation length [PC99], specially for $d = 3$ [BCF$^+$00]. Nevertheless, the FSS analysis can yield valuable information about the transition and critical exponents. We also focus the attention in the low-temperature results to check the validity of the predictions made for these parameters. In particular, we will investigate the universality at $T = 0$ as well as the scaling behaviour that will be derived in the next chapter for parameter A that vanishes $\sim TL^{-\theta}$ where θ is the thermal exponent. Moreover, in the $d = 3$ case we will find results well compatible with the conjecture that $G = 1/3$ below T_c.

The zero-temperature analysis is specially relevant in the cases of $d = 1, 2$ because these have a critical point at $T = 0$, where the correlation length diverges as $\xi \sim T^{1/\theta}$. At a critical point one has to be very careful because the limits $T \to 0$ and $V \to \infty$ do not commute. The study of G and A at low temperatures reveals that at $T = 0$ the universal values $A = 0$ and $G = 1/3$ are obtained for any finite system size. Moreover, the FSS analysis with $T_c = 0$ yields that the same correlation length exponent for A, G and B [7]. In the case when $d = 1$, OPF parameters can be computed analytically, so that all this predictions can be checked exactly. The two-dimensional case is more complex. In spite of this, from the numerical data we obtain many interesting results in agreement with the scaling predictions made in the following chapter.

The $d = 3$ nn case has been widely analysed and there is common consensus that there is a transition at finite temperature $T_c = 0.99 \pm 0.01$ [MPRL98a]. Here we address the 3 d case in the nnn version that was previously analysed with binary couplings [MPR94a]. The advantage of this model is that it has a higher transition temperature so that thermalisation is easier, while typical features at low T are expected to be the same as in the 3d nn model.

3.1 EA $d = 1$: one-dimensional Ising spin glass

The one-dimensional Ising spin chain can be solved analytically by means of the transfer matrix method [BM85]. This model is always in the paramagnetic phase and displays a second order transition at $T = 0$ where the correlation length diverges as

[7] In the two-dimensional case, the behaviour of G at low finite temperatures is not clearly defined because critical and zero temperature effects mix so that the scaling behaviour is not so clear [PRS01].

$\xi \sim 1/T$. Thus, it is an example of a system in the paramagnetic phase with OPF which in the thermodynamic limit vanish as $1/V$. Our aim here is to study analytically the behaviour of A and G. We expect that in the thermodynamic limit both parameters vanish at any temperature except at zero where $G = \frac{1}{3}$. As we have already said at a critical point the limits $V \to \infty$ and $T \to 0$ do not commute, and indeed we will see that in this model G takes the value $1/3$ at $T = 0$ for any finite system.

Consider an Ising spin glass chain with V spins and free-boundary conditions. The Hamiltonian reads,

$$\mathcal{H} = -\sum_{i=1}^{V-1} J_i \sigma_i \sigma_{i+1} \; ; \qquad \sigma_{V+1} = \sigma_1 \tag{3.41}$$

where the couplings are randomly distributed according to a probability distribution $P(J)$. The partition function being, $\mathcal{Z} = 2\prod_1^{V-1}(2\cosh[\beta J_i])$ [8] [BM85].

The easiest way to compute the average of any moment of the order parameter is to compute the generation function : $\overline{\langle e^{yq}\rangle^m}$ where m is a positive integer, q is the overlap between two different configurations of spins and the thermal average is with respect the partition function of the two-replica system,

$$\langle e^{yq}\rangle = \mathrm{Tr}_{\{\sigma\},\{\tau\}} \frac{e^{-y\,q}\, e^{-\beta(\mathcal{H}(\sigma)+\mathcal{H}(\tau))}}{\mathcal{Z}(\{\sigma\})\mathcal{Z}(\{\tau\})} \qquad q = \frac{\sum_i \sigma_i \tau_i}{V} \tag{3.42}$$

By simple partial derivation respect to y we can obtain expressions for the expectation values of all the moments of q. Hence, the terms which enter in the definition of A and G ($\overline{\langle q^2\rangle}$, $\overline{\langle q^4\rangle}$ and $\overline{\langle q^2\rangle^2}$) can be expressed as follows,

$$\overline{\langle q^n\rangle} = \frac{\partial^n \overline{\langle e^{yq}\rangle}}{\partial y^n}|_{y=0} \qquad n = 2, 4 \text{ and} \tag{3.43}$$

$$\overline{\langle q^2\rangle^2} = \frac{1}{3}\left[\frac{\partial^4 \overline{\langle e^{yq}\rangle}^2}{\partial y^4} - \frac{\partial^4 \overline{\langle e^{yq}\rangle}}{\partial y^4}\right]_{y=0} . \tag{3.44}$$

Therefore we only need to compute the generator (3.42) for $m = 1, 2$ to obtain G and A.

3.1.1 The transfer matrix method

For general m, the generator (3.42) can be computed using the transfer matrix method [Bax82, BM85]. We have to compute the average over the quenched disorder of the following object,

$$\prod_{\alpha=1}^{m} \frac{\sum_{\{\sigma^\alpha\}\{\tau^\alpha\}} \exp\left(y \sum_{i=1,V} \frac{\sigma_i^\alpha \tau_i^\alpha}{V} + \beta \sum_{i=1}^{V-1} J_i(\, \sigma_i^\alpha \sigma_{i+1}^\alpha + \tau_i^\alpha \tau_{i+1}^\alpha)\right)}{\mathcal{Z}^2} \tag{3.45}$$

[8] The model with periodic boundary conditions yields the same results when taking the limit $V \to \infty$.

where m is the number of groups of two replicas and $\alpha = 1, ..., m$ labels each group.

The average over the disorder is easily performed when we can factorise the dependence on each J_i, so that we have the product of $V-1$ identical objects. Hence, we are interested in considering the transfer matrix between two neighbouring sites, so that it contains all the dependence on the J_i. For a single pair of replicas this matrix reads,

$$\hat{t}_i \equiv \hat{t}(\sigma_i, \tau_i; \sigma_{i+1}, \tau_{i+1}) = \frac{\exp\left(y\frac{\sigma_i\tau_i+\sigma_{i+1}\tau_{i+1}}{2V} + \beta J_i(\sigma_i\sigma_{i+1} + \tau_i\tau_{i+1})\right)}{(2\cosh(\beta J_i))^2} \quad . \tag{3.46}$$

Here it is very useful to note that the number of degrees of freedom can be divided by two by noticing that $\hat{t}_i$ can be reexpressed in terms of the variable $S_i = \sigma_i\tau_i$ as follows,

$$t_i \equiv t(S_i; S_{i+1}) = \frac{1}{4}\exp\left(y\frac{S_i + S_{i+1}}{2V}\right)\left(1 + \tanh^2(\beta J_i)\ S_iS_{i+1}\right) \quad . \tag{3.47}$$

Thus we can perform the sum over one of the spin variables to obtain a global factor of $\sum_{\{\tau^\alpha\}} = 2^{V\,m}$.

For general m the matrix associated to each bond, T_i, consists of the tensorial product of m matrices t_i,

$$T_i = t_i \otimes t_i \otimes ... \otimes t_i \otimes t_i = \bigotimes_1^m t_i \tag{3.48}$$

in which the whole dependence on the coupling J_i. Averaging over the disorder yields the same contribution for every bond $\overline{T} = \overline{T_i}\ \forall i$, so that the calculation is reduced to computing,

$$\overline{\langle e^{yq}\rangle^m} = \frac{1}{4}\sum_{\{\sigma^\alpha\}\{\tau^\alpha\}} e^{y\frac{\sum_\alpha \sigma_1^\alpha\tau_1^\alpha}{2V}}\overline{T}^{V-1}e^{y\frac{\sum_\alpha \sigma_V^\alpha\tau_V^\alpha}{2V}} \quad . \tag{3.49}$$

This is equivalent to calculating the trace of the following product,

$$\overline{T}^{V-1}Q \quad , \tag{3.50}$$

where Q is a $4\ m \times 4\ m$ matrix resulting from the tensorial product of m matrices in which contains the terms of the two edges which had fallen out in the symmetrisation process,

$$Q = \bigotimes_\alpha \frac{1}{2^2}e^{y\frac{\sigma_1^\alpha\tau_1^\alpha + \sigma_V^\alpha\tau_V^\alpha}{2V}}. \tag{3.51}$$

The rest of the calculation is straightforward. In first place we have to diagonalise $\overline{T}$. Once we have obtained the set of eigenvalues and eigenvectors, in this new base we have that,

$$\overline{T}_\lambda{}^{V-1} = \begin{pmatrix} \lambda_1^{V-1} & \cdots & \cdots \\ \cdots & \lambda_2^{V-1} & \cdots \\ \cdots & \cdots & \cdots \\ \cdots & \cdots & \lambda_{2^{2m}}^{V-1} \end{pmatrix} \quad , \tag{3.52}$$

where we use the subindex λ to denote the diagonalised matrix.

The next step is to compute the change-of-base matrix, M, which expresses the new set of eigenvectors $\{\lambda^i\}$ in terms of the old base $\{\sigma^\alpha\}$. Then, the generator can be evaluated as,

$$\overline{\langle e^{yq}\rangle^m} = Tr\ M\overline{T}_\lambda{}^{V-1} M^T Q. \tag{3.53}$$

We have to point out that this computation is not easy for general m because the signalisation of T is not trivial. In Appendix B the calculations for the case $m = 1$ are done in detail and the case $m = 2$ is sketched to show which difficulties may arise. Nevertheless, we have to point out that the computation of any moment of the overlap and in particular $\overline{\langle q^2\rangle^2}$ can be done using the correlation functions $\langle\sigma_i\sigma_j\rangle$ as follows,

$$\langle q^2\rangle = \frac{1}{V} + \frac{1}{V^2}\sum_{i\neq j} T_{ij}\,; \qquad T_{ij} = \langle\sigma_i\sigma_j\rangle^2\ , \tag{3.54}$$

where in the one-dimensional case the correlations read,

$$\langle\sigma_i\sigma_j\rangle\ =\ \prod_{p=i,j-1} \tanh\beta J_p \quad i\neq j\quad . \tag{3.55}$$

3.1.2 Results

Here we report the results of the calculations in both the low-temperature and the infinite-volume limits. The outcome is that the quantities under study $\overline{\langle q^2\rangle}$, $\overline{\langle q^4\rangle}$ and $\overline{\langle q^2\rangle^2}$ only depend on V and on the following objects $\overline{R^k} \equiv \overline{(\tanh\beta J)^{2k}}$. These averages have the following behaviour in the limits of high and low temperature,

$$\overline{R^k} = \int dJ P(J)\,(\tanh\beta J)^{2k} \begin{cases} \simeq & \beta^{2k}\overline{J^{2k}} \ll 1 & \beta\to 0 \\ \simeq & 1 - a_k T P(0) \quad a_1 = 2,\ a_2 = \frac{2}{3} & \beta\to\infty \end{cases} \tag{3.56}$$

At high temperature, where $\overline{R}^V$, $\overline{R^2}^V \ll 1$ we obtain for the numerator and denominator in the definition of G (3.5),

$$\left.\begin{array}{rcl} \text{numerator} & = & \frac{4(1+\overline{R})(\overline{R}^2-\overline{R^2})}{V^3(\overline{R}-1)^3(\overline{R^2}-1)} + \mathcal{O}(\frac{1}{V^4}) \\ \text{denominator} & = & \frac{2(1+\overline{R})^2)}{V^2(1-\overline{R})^2} + \mathcal{O}(\frac{1}{V^3}) \end{array}\right\} G\ \sim\ \frac{1}{V} \tag{3.57}$$

where we have kept the lowest orders in $\frac{1}{V}$ and we have made the following approximations $\lim_{V\to\infty}\overline{R}^V, \overline{R^2}^V \to 0$. Thus as expected in a paramagnetic phase, G vanishes as $1/V$ as well as A does, since $\overline{\langle\ q^2\ \rangle}$ also goes to zero as $1/V$ (see Appendix B). In the low-temperature limit $\overline{R}, \overline{R^2} \approx 1$, from what follows that $\overline{\langle\ q^2\ \rangle} \approx 1\ +\ \mathcal{O}(T)$. Thus

the numerator and denominator in G read,

$$\text{numerator} = \frac{4D(V^4-1)T}{45V^3} + \mathcal{O}(T^2) \quad , \tag{3.58}$$

$$\text{denominator} = \frac{4D(V^4-1)T}{15V^3} + \mathcal{O}(T^2) \quad , \tag{3.59}$$

where D is given by $D = 2P(0)$. This yields $G = 1/3 + \mathcal{O}(T)$, independently of the size of the system. Note G and A take the universal values at $T = 0$ ($1/3$ and 0), despite there being a critical point where strong sample-to-sample fluctuations are known to be finite [AH96]. This happens because in second order phase transitions the limits $T \to T_c$ and $V \to \infty$ do not commute. Furthermore, we have to stress that the finite-temperature

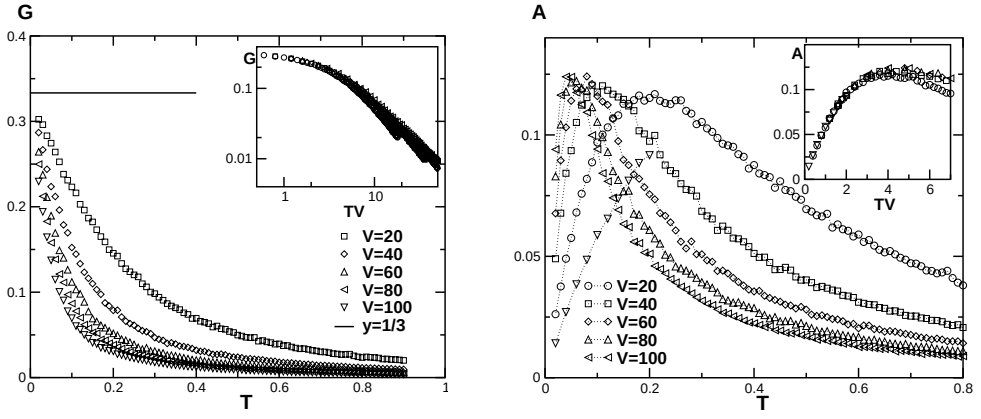

Figure 3.16. 1d EA model with Gaussian couplings: Parameter G (*left plot*) and A (*right plot*) versus temperature for system sizes $V = 2, 4, 8, 16, 32$ (from above to below). In the inset we show the scaling plot with the variable $T\,V$.

contributions to G and A scale both with system size as $T\,V$ when $V \to \infty$ (see Fig. 3.16). A detailed computation up to second order in T reveals that in the large-volume limit $G = \frac{1}{3} - \mathcal{O}(TV)$. In fact for the parameter A, we get in the limit $T \to 0$,

$$A = \frac{4D(V^4-1)T}{45V^3} + \mathcal{O}(T^2) \overset{V\to\infty}{\to} \frac{4D}{45} T\,V \quad . \tag{3.60}$$

This reflects the fact that as we get close to the transition point $T = 0$, the correlation length diverges as $\frac{1}{T}$ as we should expect from regular finite-size-scaling analysis. As we will see in the following chapter this can be derived using a low-temperature expansion in terms of excitations. Such an approach admits a scaling description of OPF at low temperatures in disordered systems with no transition at finite temperature.

3.2 EA $d = 2$

The 2d model is a more complex system which cannot be solved analytically. The first numerical studies of the the Binder cumulant showed that there was no crossing of the curves for different sizes so that there was no transition at finite temperature [BY88]. Moreover, the correlation length diverges at zero temperature as $\sim T^{-\nu}$, so that $T = 0$ is a critical point. DW studies also yielded the same conclusion, since the cost of creating a DW across a system of lattice size L vanished as L^{θ} with $\theta \approx -0.28$ [McM84d, RSB$^+$96b, HY02]. Currently, there is a consensus that this is a model with no transition at finite temperature, despite there being large finite-size effects. This huge size effects could be at the root of the discrepancies shown in the measurement of the correlation length exponent $\nu = 1/\theta$ by Monte Carlo Methods $\theta = -0.48$ [McM84a, KHS92, PRS01] and Domain Wall calculations [McM84d, RSB$^+$96b, HY02] (see for instance [Moo02, HY02]) but other interpretations are possible [PRS01]. Here we do not pretend to enter in this controversy and we content ourselves with the description of G and A in the low-temperature region.

Parameters of the simulations: we have made very precise calculations of lattices with periodic boundary conditions down to very low temperatures using transfer matrices (see Appendix C). We have averaged over 100000 samples for sizes ranging from $L = 2$ to $L = 6$.

In Fig. 3.17 we show the behaviour of B, G and A. As expected the curves do not cross at finite temperature, actually the curves for the largest sizes approach faster to zero at finite temperature as expected in a paramagnetic region. But, remarkably in both cases all the curves approach the universal value at $T = 0$, namely $G = 1/3$, $B = 1$ and $A = 0$. We meet a similar situation to that found in the 1 dimensional case, so so that close the critical point $T = 0$, B and A are functions of the scaling variable $T\ L^{-\theta=-1/\nu}$ with the same value of $\theta = -0.46$ in agreement with the findings of various authors as shown in the insets of the plots. However, note that the scaling for A only works at very low temperatures where A is linear in temperature. The reason for this finding will become clear in the next chapter where the low-temperature properties of these parameters are analysed through scaling laws. The same arguments show that the scaling for G does not work because there might not be a single exponent.

3.3 EA $d = 3$

We have numerically studied the three-dimensional EA model with nearest neighbours with Gaussian couplings. This model with a binary distribution of couplings was already studied in [MPR94a]. In this previous work the existence of a transition at finite temperature $T_c \approx 3.27$ was conjectured, but the $T = 0$ critical point could not be ruled out. Our analysis reveals that as expected there is a second order transition signalled by the crossing of all the parameters at a temperature close to 3.27. In the 3d nn case the transition temperature depends on the coupling distribution. In the literature one finds that T_c is higher when the distribution of couplings is discrete. In the nnn case, we do

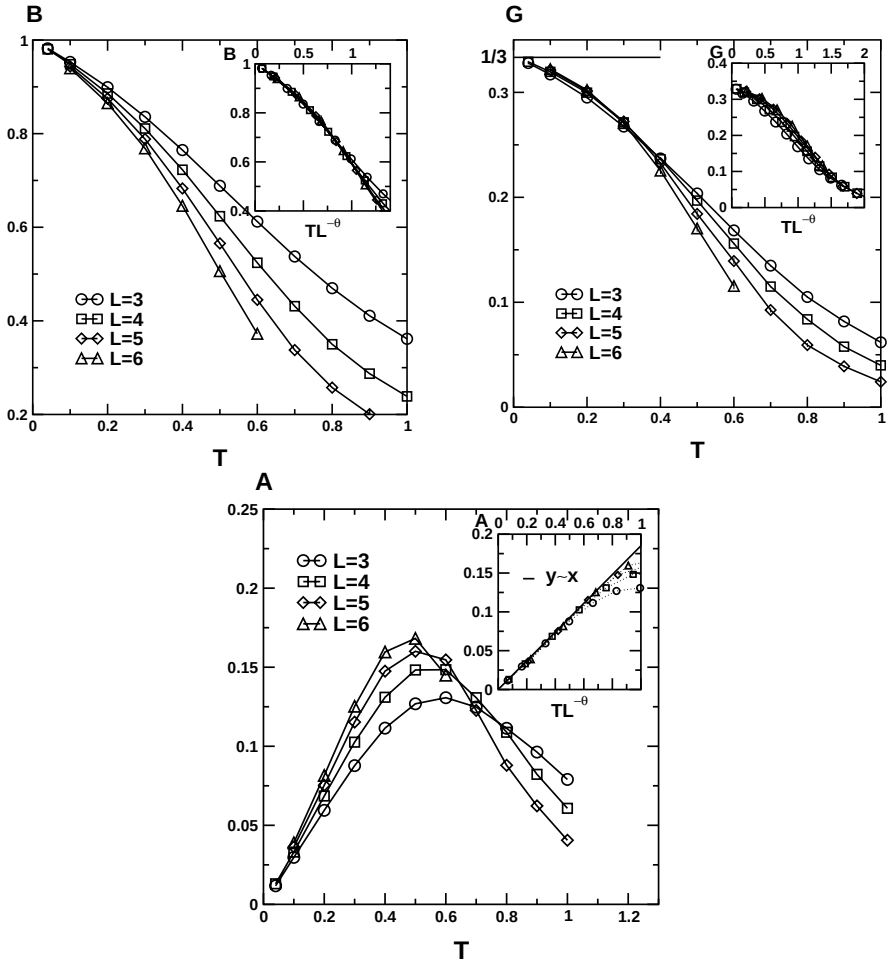

Figure 3.17. 2d EA model: Parameter B, G and A versus temperature for lattice sizes $L = 3, \cdots, 6$ from top to bottom. In each inset we show the corresponding parameter versus the scaling variable $T\ L^{-\theta}$ with $\theta = -0.46$.

not expect such differences because we expect that the number of nnn$= 26$ is enough to attenuate the differences.

Parameters of the simulations: We have studied the EA model in $d = 3$ with nnn Gaussian interactions for lattice sizes $L = 4, 5, 6, 7$. We have simulated the model in the temperature range $T = 2.5 - 5$ using the parallel tempering technique [HN96, HTY98]. The number of samples that has been used ranges from 5000 samples for the smallest size to 1250 samples for the largest one.

In Fig. 3.18 we show the numerical results obtained for B, G and A. First of all we focus the attention on the critical region. Note that the curves for different lattice

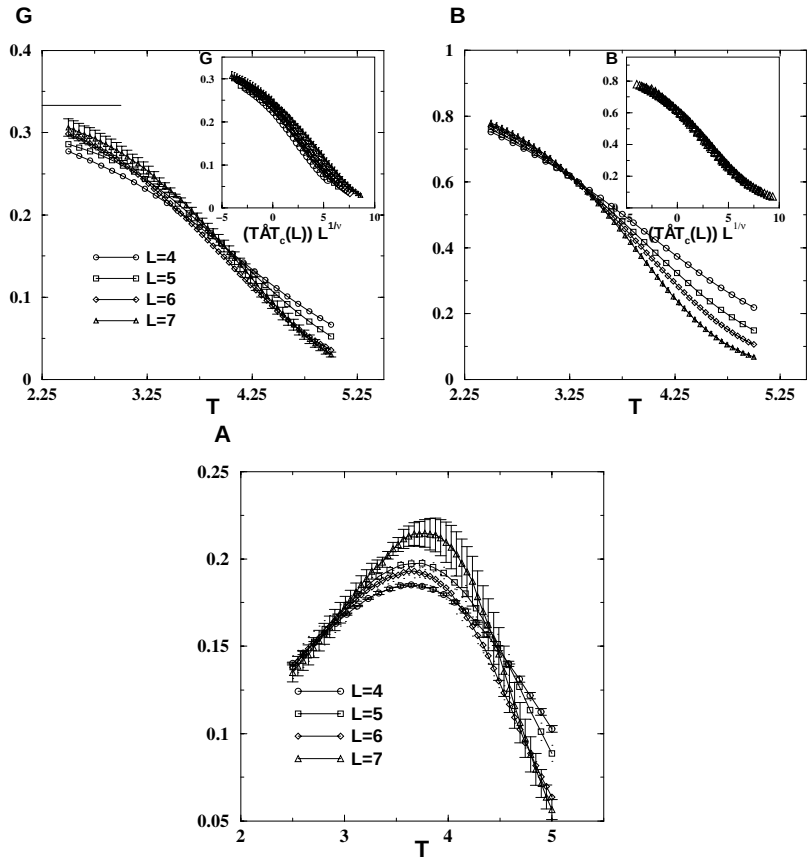

Figure 3.18. 3d nnn EA model: Parameter B, G and A versus temperature for lattice sizes $L = 4, \cdots, 7$ from bottom to top at high temperature. In the insets of G and B we show the corresponding parameter versus the scaling variable $(T - T_c(\infty))\ L^{-1/\nu}$ with $1/\nu = -0.833$ and $T_c(\infty) = 3.3$.

sizes cross signalling the existence of a continuous transition. As observed in mean-field models the corrections to T_c in the Binder parameter are of opposite sign to those of G. Despite, note that the crossing point in B is much clearer than in G. This is because OPF parameters are very sensible to rare samples so that they fluctuate a lot when the number of samples is small. This is also reflected in the scaling plots shown in the insets of the corresponding plots. We have performed the finite-size scaling analysis proposed in (3.2) for G and B with the same values for the fitting parameters $T_c(\infty)$ and ν. The best scaling corresponds to $T_c(\infty) = 3.3$ and $1/\nu = 0.833$ in agreement with the values found in the binary case. We have to remark that in (3.2) corrections to $T_c(\infty)$ are proportional to $L^{-1/\nu}$, so that if $1/\nu$ is large as in this model these corrections are too small to affect the results, even for small sizes.

The plot for A shows a maximum that for increasing system sizes approaches T_c from above as observed in the cases one and two-dimensional cases. Unfortunately, the minimum temperature reached is too high to reach any conclusion about whether A remains finite or not below T_c in the large-L limit. Nevertheless, we do observe that for increasing L the curves for G get closer to $1/3$ below T_c and that G becomes more similar to a step function supporting the conjecture that $G = 1/3$ in the frozen phase in the large-V limit. Note that this tendency is not observed in B, where for the sizes and temperatures studied curves remain very far from 1.

Chapter 4

THE SPECTRUM OF LOWEST-LYING EXCITATIONS.

The nature of *typical* excitations in short-ranged spin-glass systems is still a very controversial issue. According to the droplet theory these excitations are compact objects of linear size l, with volume $v \sim l^d$ that have a very rugged surface with a non-trivial fractal dimension $S \sim l^{d_s}$ with $d-1 < d_s < d$. The free-energy cost of creating this droplet is $\sim l^\theta$, thus, only if $\theta \geq 0$ the spin-glass order is stable at finite temperature. Another possibility is that excitations are described at least up to a certain extent by MFT. According to it, large size excitations have a free-energy cost of $\mathcal{O}(1)$ in the thermodynamic limit, so that $\theta = 0$, and as they fill the whole space the surface is fractal with $d_s = d-1$.

Numerically, the usual approach is to find a numerical method capable of creating a *typical excitation* in order to estimate the thermal exponent, θ. The first attempt was the domain wall method introduced by McMillan for 2d EA spin glasses [McM84c] (see Sec. 2.3.1). The purpose of this method is to evaluate at $T = 0$ the energy cost of creating a domain wall across a system of size L. This energy cost is assumed to scale with system size as $\sim L^\theta$. This analysis yields a lower critical dimension is somewhere between $d = 2$ and 3. Studies in 2d yield $\theta \approx -.28$ [McM84c, BM84, RSB$^+$96b, PY99, HY01, CBM01, PRS01] so that there is no transition at finite temperature; whereas $\theta > 0$ in 3 and 4 dimensions: $\theta(3d) \approx 0.2$ [BM84, McM84b, PY00b, Har99b] and $\theta(4d) \approx 0.7$ [Har99a, Huk99] meaning that there is no RSB at low temperature. However, the interpretation of Domain Wall results has become very controversial because it is not clear that a DW created in a system of linear size L can be identified with the active droplet at this same length scale [LBMM02, PRS01, HY02]. The key argument is that geometrically a DW excitation is very different from a droplet because the former is essentially an elastic line of broken bonds that crosses the system along one of its directions whereas the latter has to close on itself. The droplet theory argues that these effects disappear with system size [Moo02]. However, already in two dimensions, studies using different techniques that are supposed to excite droplets rather than DW such as Monte Carlo simulations at low temperature or $T = 0$ analysis introducing magnetic field

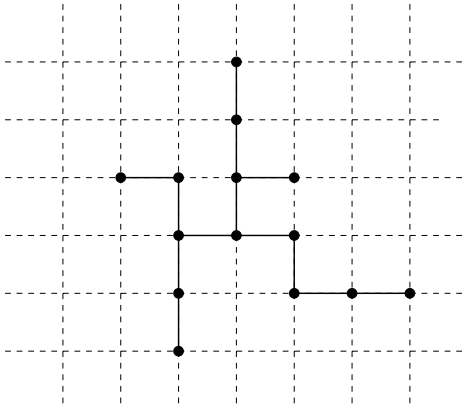

Figure 4.1. Schematic picture of a lattice animal in a two-dimensional lattice. Note that all the sites belonging to this kind of cluster belong, as well, to the surface, so that $v \sim S$.

perturbations, yield very different estimates for the θ exponent, $\theta \approx -0.47$ [KHS92, KS92, RSB$^+$96b] that does not seem to converge to the DW value for larger lattice sizes. This has motivated the search for other methods that introduce a perturbation to the original ground state that brings about excitations that occupy a finite fraction of the spins in the system [PY00a, KM00]. The outcome of numerical studies in three and four dimensions has put forward a new intermediate picture known as TNT scenario (that stands for trivial-non-trivial) [PY00a, KM00] in which droplets have a fractal surface but their energy cost does not scale with system size so that $\theta = 0$ as in MFT. These results have been confirmed by MC simulations at very low temperature (and thus not affected by criticality) [KPY01]. All the same, system sizes numerically available are very limited ($L < 20$) so that there could well be large finite-size effects affecting these results. Still, recent investigations that look for the cluster of minimum energy that contains a certain number of spins including a fixed central spin, show that these excitations are not compact objects but lattice animals (see Fig. 4.1) and that θ is small and slightly negative which is at large discrepancy with the classical droplet description and DW results [LBMM02]. All these results suggest that maybe the droplet picture should be modified to give a more correct picture of excitations in short-ranged systems.

Here we propose an alternative approach valid only for systems with no accidental degeneracy of the ground state. The idea is to study the low-temperature behaviour starting from the analysis of the first excitations. These are the excitations which are *closest in energy to the ground state* and are not necessarily typical. At higher temperature there might be other excitations more favoured entropically whose contribution to the free-energy has a larger weight. Notwithstanding this, we argue that from the study of this lowest-lying excitations we can infer many properties about the low-temperature phase, in particular the scaling properties of $T = 0$ fixed point. Actually, by assuming

a particular scaling ansatz for the distribution of volumes and energy costs, we can describe excitations through the *lowest-droplet* (for lowest-lying excitations) exponents (θ_l and λ_l). From these, we can gain valuable information about the finite-T behaviour of any quantity related to the $P(q)$ from which we can evaluate the thermal exponent, θ. In particular, under very mild assumptions such as the uniqueness of the ground state and the finite probability of having an excitation at zero cost, the universal values at $T = 0$ for OPF parameters can be recovered. Moreover, based on numerical results, we propose a scenario for the excitation spectrum in which energy levels are random uncorrelated variables independent of the size of the excitation. This description is useful to understand the low-temperature behaviour of thermal quantities such as the specific heat that will turn out to depend exclusively in the exponent characterising the energy cost of lowest excitations, θ_l.

In our analysis we will not make any particular assumption on what are the properties of the surface of excitations which could be fractal or not. But we expect that a similar analysis could be carried out for the *link-overlap*: $q_\ell = \frac{2}{V(V-2)} \sum_{(i \neq j)} S_i^a S_j^a S_i^b S_j^b$ and its distribution in which the information about the surface of droplets is contained.

The theoretical predictions will be checked with the numerical study of the first excitations of different models such as the EA in 1 and 2 dimensions and the study of the SK model.

1. Lowest-excitation expansion

The aim is to study the properties close to $T = 0$ considering the ground state and the lowest-lying excitation. We start from the most general Hamiltonian for a system of V Ising spins,

$$\mathcal{H} = -\sum_{i,j} J_{ij} S_i S_j \quad , \tag{4.1}$$

where the J_{ij} can be either 0 (depending on the dimensionality and interaction range of the system) or distributed according to some continuous $P(J)$ [1]. If the coupling distribution is continuous, there is a unique ground state (up to a global flip of all the spins), whose configuration we denote by $\{S_i^*\}$. This Hamiltonian can be rewritten in terms of local fields, $\mathcal{H} = -\sum_i h_i S_i$, such that each local field reads, $h_i = \frac{1}{2} \sum_{j \neq i} J_{ij} S_j$. In the ground-state configuration each spin S_i is aligned with its local field h_i, so that the ground-state energy is $E_{\rm GS} = -\sum_i h_i^* S_i^* = -\sum_i |h_i^*| = -\sum_{i,j} J_{ij} S_i^* S_j^*$.

Suppose that for a given sample we know the ground-state configuration $\{S_i^*\}$. Consider now an excitation of volume v such that all excited spins are connected to each other, this is what we call a *cluster* (see Fig. 4.2). In this new state, v spins will change their orientation with respect to the ground-state configuration, hence the overlap between these two states is $q_v = 1 - \frac{2v}{V}$. The energy cost ΔE of this excitation depends only on

[1] This Hamiltonian is rather general so that the conclusions that are drawn here could be valid in general for any Ising spin system, but not necessarily for continuous spin models.

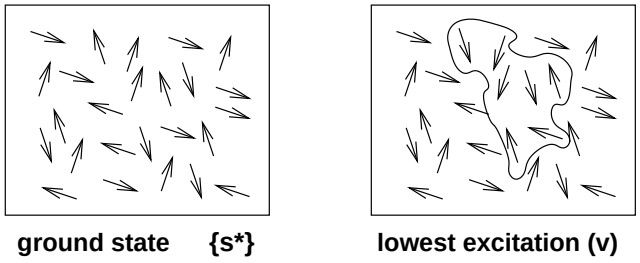

Figure 4.2. Schematic picture of the ground state and its corresponding lowest-lying excitation which is a *cluster*.

the bonds broken at the surface,

$$\Delta E = 2 \sum_{\mathrm{ik} \in \mathrm{surface}} J_{i,k} S_i^* S_k^* \quad , \tag{4.2}$$

where each coupling is counted only once. The minimum cost excitation is always a cluster, because an excitation consisting in two or more disconnected clusters necessarily costs more energy than reverting a single one. The lowest excitation with energy $\epsilon = \Delta E^*$ corresponds to breaking a subset of bonds among the $\{J_{i,k}\}$ such that the value in (4.2) is minimum.

In general, the size v and energy cost ϵ of a lowest-lying excitation are random variables depending on the sample. Since there might be correlations between the local fields that enhance clusters of a certain size, we assume that clusters of any size v can take place with a finite probability g_v that is normalised $\sum_v g_v = 1$. Note that for systems with TRS, $g_v = g_{V-v}$. For each excitation volume there is a distribution of energy costs ϵ that depends on v: $P_v(\epsilon),\ \epsilon \in [0, \infty)$, such that $\int_0^\infty d\epsilon P_v(\epsilon) = 1, , \forall v$. Therefore, the probability of having an excitation with energy cost ϵ and a volume v reads,

$$\mathcal{P}(v, \epsilon) = g_v \ P_v(\epsilon) \ ; \qquad \sum_v \int_0^\infty d\epsilon g_v \ P_v(\epsilon) = 1 \ . \tag{4.3}$$

At very low temperature, we will assume that the partition function can be approximated by the ground state plus the first excitation, $\mathcal{Z} = e^{-\beta E_{\mathrm{GS}}} \left(1 + e^{-\beta\epsilon}\right)$. Averaging over all samples we obtain the following expression for the free-energy,

$$\overline{\beta F} = -\overline{\ln \mathcal{Z}} = \overline{\beta E_{\mathrm{GS}}} - \overline{\ln\left[1 + e^{-\beta\epsilon}\right]} \stackrel{\beta\to\infty}{\longrightarrow} E_{\mathrm{GS}} - \frac{\pi^2}{12} T \sum_v \mathcal{P}(v, 0) \tag{4.4}$$

To compute the low-temperature limit of the disorder average in (4.4) we have introduced the variable $x = \beta\epsilon$,

$$\overline{\ln\left[1 + e^{-\beta\epsilon}\right]} \quad = \quad \sum_v \int_0^\infty d\epsilon \ \mathcal{P}(v, \epsilon) \ln\left[1 + e^{-\beta\epsilon}\right]$$

$$
\begin{aligned}
&= T\sum_v \int_0^\infty dx\ \mathcal{P}(v,\frac{x}{\beta})\ln\left[1+e^{-x}\right] \\
&\stackrel{\beta\to\infty}{\longrightarrow} T\sum_v \mathcal{P}(v,0)\int_0^\infty dx \ln\left[1+e^{-x}\right] + \mathcal{O}(T^2) \\
&= \frac{\pi^2}{12}\,T\,\sum_v \mathcal{P}(v,0) + \mathcal{O}(T^2)\ . \qquad (4.5)
\end{aligned}
$$

Therefore, at low temperature the leading behaviour in T is given by the lowest-lying excitations provided the weight of having an excitation with no energy gap $\sum_v \mathcal{P}(v,0)$ is finite. Considering excitations occupying a higher level in the spectrum $p = 2, 3, \cdots$, would result in contributions of order $T^p,\ p = 2, 3, \cdots$.

The validity of the first-excitation expansion can be justified according to the following argument. Consider a very large system. Due to frustration there will exist many excitations nearly degenerate with the ground state with a broad distribution of sizes. In this situation, a priori, one should consider the contribution to the partition function of all these excited states. Suppose that we take the ground state configuration and we split the system in a large number of smaller subsystems in such a way that in the infinite-volume limit, these systems are also large. Each of these subsystems has one ground state and its own spectrum of excited states. Since the ground-state configuration is that of the global ground state, the first excitation of each subsystem corresponds necessarily to a lowest-lying excitation in the spectrum of the original system. Therefore, since we have a large number of subsystems, the spectrum of excitations of a large sample is roughly described by the first excitations of all the subsystems. Of course, huge excitations of a size larger that that of a subsystem are not included, but in the thermodynamic limit the first excitation of a single subsystem can be large enough to occupy a finite fraction of spins of the original system. Hence, if excitations are random, the thermal average over all the lowest-lying excitations is equivalent to the average over the first excitations of a large number of subsystems. Certainly, in this argument we have considered very special boundary conditions for each subsystem. Nevertheless, we do not expect that typical properties depend on the particular choice of the boundary conditions, thus the same argument holds for independent subsystems. Despite the fact that the local ground-state configuration of each independent subsystem might be different from the original one, it still will correspond to one of the low-lying excitations of the spectrum and the same would apply for the first excitation.

Another possibility, specially for systems with $\theta > 0$ which only allow for small-size excitations, would be to perform an expansion in terms of clusters of different sizes in the same spirit as in ferromagnets [CL95]. In the ground-state configuration of a ferromagnet, the spins point in the same direction so that $E_{\rm GS} = -\ n_c\ J\ V$ where n_c is the coordination number ($2d$ in a cubic lattice) and J is the coupling constant. The lowest-lying excitation is generated by overturning a single spin at a cost of $\epsilon = 4Jd > 0$. Thus there are V lowest excitations which yield the same contribution to the free-energy

that vanishes exponentially at low temperature [2],

$$\beta F = \beta E_{\rm GS} - T \ln \left[1 + V e^{-\beta 4 d J} \right] \quad . \tag{4.6}$$

This is the usual situation in ordered systems with gap. However, in a spin glass with $\theta > 0$ the situation is different. If we consider all possible one-spin excitations, these have an energy cost $\epsilon_i = 2\ h_i$. Since in a finite-dimensional system the local-field distribution has a finite weight at zero field $P_1(h_i = 0) > 0$ [PP79], the contribution to the free-energy vanishes algebraically at low temperature and reads,

$$\overline{\beta\, F} = \overline{\beta\, E_{\rm GS}} - T\ V\ P_1(0)\ \frac{\pi^2}{12} + \mathcal{O}(T^2) \tag{4.7}$$

However, we note that considering bigger clusters such as two neighbouring spins would yield also contributions linear in T provided the weight of having such an excitation with zero energy cost is finite. This assumption is reasonable because local fields can have short-ranged correlations enhancing these small-scale droplets. In this situation one should propose a certain ansatz for each energy distribution and a simplified analysis is not easy so that we will not discuss this case in detail. Nevertheless, we will see that most of the results reported below are also obtained if we consider only one-spin excitations with a finite probability at zero local field.

The scaling ansatz and the uncorrelated energy-size scenario

It is specially interesting to analyse the behaviour when excitations scale with system size $v = \mathcal{O}(V)$ because these excitations are supposed to yield the relevant contribution to the thermodynamics. We characterise the probability distribution $\mathcal{P}(v, \epsilon)$ of large excitations with two exponents that we shall call *lowest-droplet* exponents: θ_l and λ_l.

- Lowest-droplet exponent: θ_l
  This exponent describes the scaling behaviour of the distribution of energy costs. Assuming that an excitation of volume v has a linear dimension l such that $v = l^d$ we suppose that the weight at zero cost scales as $P_v(0) \sim l^{\theta_l}$, $\theta_l < 0$ so that,

$$P_v(\epsilon) = l^{-\theta_l} \hat{P} \left(\frac{\epsilon}{l^{\theta_l}} \right)\ ;\ \hat{P}(0) > 0\ . \tag{4.8}$$

  In particular, for finite-dimensional systems we expect that $\theta_l \leq -d$, as one-spin excitations (which are not necessarily the excitations with the smallest energy gap) yield an upper bound (ub) for the energy cost of the lowest excitation, $\theta_l \leq {\theta_l}^{\rm ub}$. The statistics of one-spin excitations is governed by the behaviour of the ground-state local-field distribution $G(\{h_i\})$ in the limit $h \to 0$. In a finite-dimensional

[2] In a random ferromagnet where the couplings are distributed according to a $P(J)$, $J \in [0, \infty)$ the situation is the same because $\mathcal{P}(\epsilon = 0) = 0$.

system if the couplings are continuously distributed, the local fields can be considered as independent random variables, so that the whole local-field distribution can be assumed to be self-averaging $G(\{h_i\}) = \prod_i P_1(h_i)$ where $P_1(h_i)$ is the single-site local-field distribution that has a finite weight at zero field, $P_1(0) > 0$ [PP79]. The probability of having a lowest excitation of cost $\sim h$ among the V excitations is $VP_1(h' < h)$, where $P_1(h' < h) = \int_0^h dh' P_1(h')$. The characteristic energy $h^*(V)$ is that associated to an excitation that happens with probability one so that $VP(h' < h^*(V)) = 1$. From here it follows that the characteristic energy scales as $h^*(V) \sim 1/(V P_1(0))$ yielding $\theta_l{}^{\rm ub} = -d$, hence $\theta_l \leq -d$. In mean-field models such as the SK model, the single-site local-field distribution is not an exponential but vanishes for small local fields as a power law: $P(h \to 0) \sim h^\eta$, $\eta \geq 1$ [MPV87]. Under the assumption that the whole local field distribution is SA, the characteristic energy of the lowest-lying one-spin excitation scales as $V^{-1/(\eta+1)}$.

- Lowest-droplet exponent: λ_l
  This exponent describes the probability of having a lowest excitation that spans the whole system. The number of possible one-spin excitations, $\mathcal{N}_1$, in a system of volume V is $\mathcal{N}_1 = V$. In a finite-dimensional system we expect that the number of compact clusters of any finite size v is also proportional to system size, $\mathcal{N}_v \sim V$. The probability of the lowest-energy cluster of a certain size scales roughly as $1/\mathcal{N}_v$, hence volume distribution of low-energy compact clusters should scale as $g_v = 1/V\, f(v/V)$. Nonetheless, first excitations are not necessarily compact clusters but can have a fractal surface dimension. Therefore, in general, the number of clusters of $v = \mathcal{O}(V)$ is much larger [3], so that we will assume that the distribution of large-scale excitations scales as $g_v \sim 1/V^{\lambda_l+1}$ with $\lambda_l \geq 0$. In general, it is easier to work in terms of the overlap $q = 1 - 2v/V$ so that $g_v = 2/V\, g(q)$ and $\int_0^{1-2/V} dq\, g(q) = 1$ [4],

$$g_v = \frac{1}{V^{\lambda_l+1}} \hat{g}(q)\,; \qquad g(q) = \frac{2}{V^{\lambda_l}} \hat{g}(q) \ . \tag{4.9}$$

  Note that to ensure the normalisation condition for g_v, the probability of having finite-size excitations $v = \mathcal{O}(1)$ is $g_v \approx 1 - \mathcal{O}(V^{\lambda_l})$, which is positive because $\lambda_l \geq 0$. Since excitations can be of any size, the average volume of excitations scales as $\overline{v} \sim L^{d(1-\lambda_l)}$. Hence, if $\lambda_l > 1$, the average volume is $\mathcal{O}(1)$. Note that we have not made any assumption about how is the whole distribution of excitation volumes. However it turns out that in all the models under study a single exponent λ_l describes the behaviour of both small ($v = \mathcal{O}(1)$) and large excitations ($v \sim V$).

[3] Note that this argument is valid for short-ranged systems. Nevertheless, in mean-field models this assumption also holds even though all clusters are compact by construction.

[4] Note that the upper limit in this integral is set by the size of the smallest excitation, *i.e.* one-spin excitations with $v = 1 \to q = 1 - 2/V$, which corresponds to 1 in the large-V limit.

Within this ansatz the probability of having a system-size excitation ($v \sim V = L^d$) with energy cost ϵ scales as,

$$\mathcal{P}(v,\epsilon) \sim L^{-\theta_l - d\ \lambda_l} \quad . \tag{4.10}$$

We expect that at finite temperature large-scale excitations contribute to equilibrium properties with this probability, so that we identify this combination of exponents with the thermal exponent in the droplet description for spin glasses, $\theta = \theta_l + d\ \lambda_l$. In this picture it is considered that the relevant contribution to the physics at finite temperature is given by *typical* excitations that have a cost in free-energy $\sim L^\theta$ and thus take place with a probability $\sim L^{-\theta}$.

The properties of the spectrum of excitations are described by the *uncorrelated energy-size scenario* which is based on two assumptions: *i:* correlations between energy gaps of different excitations vanish in the limit $L \to \infty$ and *ii:* correlations between excitation volumes v_i and gaps ϵ_i vanish in the thermodynamic limit, where the subindex i denotes different levels in the spectrum. This last assumption means that $P_v(\epsilon)$ is independent of v, so that $P(\epsilon) = P_v(\epsilon)$, $\forall v$. These two assumptions appear rather natural in a random system where frustration plays an important role such as a spin glass [5]. Because there exist large excitations that are very different to the ground state but very close in energy, we expect that the statistics of the energy separating the first and the second excitation is the same as that corresponding to the first excitation. From what follows that the statistics of the whole spectrum does not change if we drop off the ground state. Note that here we consider that neither excitation volumes nor gaps depend on the particular energy level of the excitation, but that there could be correlations between the volumes of different excitations. These assumptions are not valid in an ordered system where the ground state follows an ordered pattern and large-scale excitations are not statistically represented by the lowest ones.

1.1 Thermal properties: the specific heat

In Sec. 1.1 we have already pointed out that the specific heat of spin glasses and other systems such as amorphous materials and glasses vanishes linearly with temperature. This is usually associated with a finite density of states at zero gap. Due to the simplicity of this result very few attention has been devoted to this question both experimentally and theoretically. Here, we show that the behaviour of the specific heat at low temperature depends on the value of θ_l and yields interesting information about finite-volume effects.

The starting point is the expression given for the free-energy at low temperature. The terms contributing to the free-energy in (4.4) depend on the distribution of excitations only through the term $\sum_v g_v P_v(0)$. We are going to show that if we consider the contributions coming from second and higher excitations we encounter the same situation. For instance, consider the two lowest excitations. These will be clusters of energies $\epsilon_1,\ \epsilon_2,\ (\epsilon_2 > \epsilon_1)$

[5] These assumptions have been checked in the 1d, 2d EA models [PRS01] as well as in mean-field models [RS02].

and volumes $v_1,\ v_2$ with a certain overlapping volume u described by the probability [6],

$$\mathcal{P}(v_1, v_2, u; \epsilon_1, \epsilon_2) = g_{v_1,v_2,u}\ P_{v_1,v_2,u}(\epsilon_1, \epsilon_2) \tag{4.11}$$

This probability is related to the probability distribution of the lowest-lying excitation by integrating out the variables corresponding to the second excitation, $\mathcal{P}(v_1; \epsilon_1) = \sum_{v_2,u} \int_{\epsilon_1}^{\infty} d\epsilon_2\, \mathcal{P}(v_1, v_2, u; \epsilon_1, \epsilon_2)$. Following the same steps as in (4.5) we obtain that the free-energy at low temperature can be expanded in powers of T,

$$\begin{aligned} \overline{\beta F} &= \overline{\beta E_{\rm gs}} - \frac{\pi^2}{12}\, T\, \sum_v g_v P_v(0) - \frac{3\ \zeta[3]}{4}\, T^2\, \sum_{v_1} g_{v_1} P'_{v_1}(0) \\ &- K\ T^2 \sum_{v_1,v_2,u} \mathcal{P}(v_1, v_2, u; 0, 0) \quad , \end{aligned} \tag{4.12}$$

where $\zeta[s] = \sum_{k=1}^{\infty} k^s$ is the Riemann function and $P'_{v_1}(0) = \partial P(\epsilon)/\partial\epsilon|_{\epsilon=0}$. K is a constant given by a lengthy expression that can be numerically evaluated $K \approx 0.12927$ [7].

In the uncorrelated energy-size scenario the distribution of energy gaps becomes independent of the excitation volumes so that $P_v(E) = P^{(1)}(E),\ \forall v$, where we have introduced the label (1) to denote single-level distributions. Hence, as the g_v's are normalised all the terms in (4.12) become volume independent. Moreover, since there are no correlations between energy gaps the whole distribution function of p gaps factorises in the thermodynamic limit: $\mathcal{P}^{(p)}(E_1, \cdots, E_p) = \prod_i P_i^{(1)}(E_i)$, where all the $P_i^{(1)}(E_i)$'s scale with the same exponent θ_l (4.8). Hence, the different terms in the expression for βF (4.12) yield the following contributions,

$$\mathcal{O}(T): \qquad P_{v_1}(0) = P^{(1)}(0) \sim L^{-\theta_l} \tag{4.13}$$

$$\mathcal{O}(T^2): \qquad P'_{v_1}(0) \sim L^{-2\,\theta_l},\ P_{v_1,v_2,u}(0,0) = \mathcal{P}^{(2)}(0,0) \sim L^{-2\,\theta_l} \quad . \tag{4.14}$$

Therefore all the terms in (4.12) depend on the variable $T\ L^{-\theta_l}$. This expansion can be extended to higher orders in T by considering excitations higher in the spectrum. The contributions at order T^p come from terms of the type $\nabla^r_{(E_1;r_1),\cdots,(E_u;r_u)} \mathcal{P}^x(E_1, \cdots, E_v)$ such that $r = \sum_i r_i$ and $p = r + x$. Here ∇^r corresponds to the generalised derivative of a function of x variables. The derivative with respect to variable i is taken r_i times, so that the total number of derivatives is r. In virtue of the preceding assumptions, this yields the following contribution at zero energy cost: $L^{-\theta_l(\sum r_i + v) = \theta_l r}$.

From here it follows that specific heat $c = \beta^2/V(\partial^2(\beta F)/\partial^2\beta)$ at low temperature is, as well, a function of the variable $x = TL^{-\theta_l}$, so that we can express c in terms of a

---

[6] This probability is also suitably normalised: $\sum_{v_1,v_2,u} g_{v_1,v_2,u} = 1$, $\int_0^\infty d\epsilon_1 \int_0^\infty d\epsilon_2 P_{v_1,v_2,u}(\epsilon_1, \epsilon_2) = 1\ \forall v_1, v, u$
$\Longrightarrow \sum_{v_1,v_2,u} \int_0^\infty d\epsilon_1 \int_0^\infty d\epsilon_2 \mathcal{P}(v_1, v_2, u; \epsilon_1, \epsilon_2) = 1.$

[7] $K = -\frac{1}{3}\ln[3]^2 + \frac{1}{2}\ln[3]\,(\mathrm{Li}_2[1/9] - 6\,\mathrm{Li}_2[1/3]) - \frac{4}{3}\mathrm{Li}_3[-1/2] + \frac{1}{4}\,(\mathrm{Li}_3[1/9] - 12\,\mathrm{Li}_3[1/3] + 7\zeta[3]) \approx 0.1293$ where $\mathrm{Li}_s[z] = \sum_{k=1}^{\infty} z^k/k^s$ is the polylogarithm function.

scaling function $\hat{c}(x)$,

$$c = \frac{1}{V}\left(a_1 T L^{-\theta_l} + a_2\left(TL^{-\theta_l}\right)^2 + \cdots + a_n\left(TL^{-\theta_l}\right)^n\right) \to c = \frac{1}{V}\hat{c}\left(TL^{-\theta_l}\right)$$
$$a_1 = \frac{\pi^2}{12}\hat{P}^{(1)}(0)\,; \qquad a_2 = \frac{9\zeta[3]}{2}P'^{(1)}(0) + 6\,K\,P^{(2)}(0,0) \tag{4.15}$$

This is a situation similar to critical phenomena. In the scaling region $TL^{-\theta_l} < 1$ the heat capacity is finite and vanishes at $T = 0$. However, the limits $T \to 0$ and $V \to \infty$ do not commute. In the thermodynamic limit because $\theta_l < 0$, this leads to an apparent divergent series. Nevertheless, we expect that the specific heat is finite at low temperature. As in ordinary critical phenomena this is achieved assuming that in the large x limit , $\hat{c}(x)$ diverges as a power law : $\hat{c}(x) \sim x^\alpha$ in such a way that the dependence of c on L vanishes. With these considerations we read off $\alpha = -d/\theta_l$, so that the specific heat vanishes as $c \sim T^{-d/\theta_l}$. Therefore the singular function $\hat{c}(x)$ has these two limiting behaviours $\hat{c}(x) \sim x$, $x \ll 1$ and $\hat{c}(x) \sim x^\alpha$, $x \to \infty$. This implies that the specific heat is linear at low temperature provided $\theta_l = -d$. (This is the value of θ_l that one expects from the analysis statistics of one-spin excitations in finite-dimensional systems). However, it turns out that θ_l has very large finite-size corrections which are not only consequence of the finite-volume corrections that affect the statistics of one-spin excitations, but to finite volume corrections to the whole distribution of excitations. For finite L we have to use effective exponents to describe the energy cost distribution such that $|\theta_l^{\rm eff}| < d$. Thus, the heat capacity is a function of $TL^{-\theta_{\rm eff}}$ and displays a crossover from a linear regime to a regime where c behaves as a power law with an exponent slightly bigger that one, $\hat{c} \sim T^{1+\alpha'(L)}$. Note that we have introduced the *specific heat anomaly* ($\alpha'(L) > 0$) to account for deviations from linearity that, however, must vanish in the thermodynamic limit when again the linear behaviour is recovered. Thus, the measure of the specific heat at low temperatures is a useful tool to evaluate the magnitude of the finite-size corrections to θ_l energy, which as far as we know are very difficult to control.

In a mean-field model there is no dimension, so that the expansion has to be made in terms of $TV^{-\alpha}$, $\alpha = \theta_l/d$. We will see that in the SK model the analysis of lowest-lying excitations yields $\theta_l = -0.5$ ad $c \sim T^2$ as expected from MFT results [MPV87].

1.2 The $P(q)$ at low temperature

The lowest-lying expansion also lets us make instructive connections between the distribution of excitation volumes $g(q)$ and the $P(q)$. Note that in the previous analysis, we have not made any particular assumption on the scaling form of $g_{v_1,v_2,u}$, which due to the existence of correlations between volumes does not factorise. Thus, in general, it scales as $g_{v_1,v_2,u} \sim V^{-2(1+\lambda_l)-1-\rho}$ where we have introduced $\rho > 0$ to take into account correlations. This yields the analysis of overlap-related quantities more complicated, but still one can learn several things from the contributions linear in T.

If we consider two identical copies σ and τ of the system we can compute the $P_J(q)$ as follows,

$$P_J(q) = \sum_{\{\sigma\},\{\tau\}} \frac{\delta(q - q_{\sigma\tau}) e^{-\beta(\mathcal{H}(\sigma)+\mathcal{H}(\tau))}}{\mathcal{Z}^2} \tag{4.16}$$

The overlap between the excited state and the ground state is $q_v = 1 - \frac{2v}{V}$. Then, the overlap between the two replicas $q_{\sigma\tau}$ can take two possible values: *i)* $q_{\sigma\tau} = 1$ if both replicas are in the same state (either the ground state or the excited state) or *ii)* $q_{\sigma\tau} = q_v$ if one replica is in the ground state and the other one is in the excited state. Therefore, the $P_J(q)$ reads,

$$P_J(q) = \delta(q-1)\,(1-2x) + \delta(q-q_v)\;2x\;, \qquad x \equiv \frac{e^{-\beta\epsilon}}{\mathcal{Z}^2} \tag{4.17}$$

The average over the disorder of the $P_J(q)$ yields in the limit $T \to 0$ the following expression for the $P(q)$,

$$P(q) = \overline{P_J(q)} = \delta(q-1)\left(1 - T\sum_v g_v\; P_v(0)\right) + \; T\sum_v g_v\; P_v(0)\;\delta(q-q_v)\;. \tag{4.18}$$

In this expression, there are several points worth commenting on. First, note that at zero temperature the $P(q) = \delta(q-1)$ [8] as expected [PY00a, KM01]. Second, at finite temperature the $P(q)$ becomes a non-trivial function of q if the term $\sum_v g_v\; P_v(0)\delta(q-q_v)$ is finite. In particular we are interested in the contributions coming from large excitations with $q \approx 0$. The contribution of these excitations scales as $TL^{-\theta}$ so that there is RSB if $\theta = 0$ [9]. In this case, under the random-energy level scenario this amounts to say that the $g(q)$ contains all the information about the $P(q)$ at low temperature,

$$\begin{aligned}\sum_v g_v\; P_v(0)\delta(q-q_v) &= \frac{\mathcal{P}^{(1)}(0)}{2}\int_0^1 dq'\; g(q')\delta(q-q') \\ &\overset{v=\mathcal{O}(V)}{\to}\; \frac{\mathcal{P}^{(1)}(0)}{V^{\lambda_l}} g(q) \sim TL^{-\theta_l - d\,\lambda_l}\;,\end{aligned} \tag{4.19}$$

where in the last step we have used the scaling ansätze (4.8) and (4.9). Thus, with the analysis of the lowest-lying excitations we have reached the same conclusion as in standard droplet theory and, in addition, we have learnt how we can obtain information about the $P(q)$ from the statistics of the lowest-lying excitations by measuring the $g(q)$.

[8] Here we are considering that the system is time-reversal symmetric, which amounts to constrain the averages to the states for which $q > 0$. In expression (4.18) we compute $P_+(q)$, to compute the total $P(q)$ we should consider the configurations corresponding to a global flip of all the spins in both configurations, that of the ground state and that of the excited state. Thus the $P(q)$ would read $P(q) = \frac{1}{2}P_+(q) + \frac{1}{2}P_-(q)$.

[9] This result had been previously derived by Young and Reger [RY88].

1.2.1 OPF at low temperatures

We can go further on in this analysis and compute the probability distribution of two overlaps $P(q,q') = \overline{P_J(q)\ P_J(q')}$. This will be very useful to analyse OPF at low temperature. And, more specifically, to show that the sum rule in (3.7) leading to the universal value $G = 1/3$ at $T = 0$ holds at $\mathcal{O}(T)$ provided there is a finite weight at zero gap.

From the expression of the $P_J(q)$ in (4.18) we obtain the following average distribution of two overlaps in the low-temperature limit,

$$\begin{aligned} P(q,q') &= \delta(q-1)\ \delta(q'-1)\left(1-\frac{5}{3}T\sum_v g_v P_v(0)\right) \\ &+ \frac{1}{3}T\sum_v g_v P_v(0)\ \left[\delta(q-q_v)\ \delta(q'-1)+\delta(q'-q_v)\ \delta(q-1)\right] \\ &+ \frac{2}{3}T\sum_v g_v P_v(0)\ \delta(q-q_v)\ \delta(q'-q_v) \end{aligned} \tag{4.20}$$

The sum rule (3.7) states that $P(q,q') = \frac{1}{3}P(q)\ \delta(q-q') + \frac{2}{3}\ P(q)\ P(q')$. From the expression of the $P(q)$ in (4.18) we obtain up to order T,

$$\begin{aligned} P(q)\delta(q-q') &= \delta(q-1)\ \delta(q'-1)\ \left(1-T\sum_v P_v(0)\, g_v\right) \\ &+ \sum_v P_v(0)\, g_v \delta(q-q_v)\ \delta(q'-q_v) + \mathcal{O}(T^2) \end{aligned} \tag{4.21}$$

$$\begin{aligned} P(q)P(q') &= \delta(q-1)\ \delta(q'-1)\ \left(1-2\ T\sum_v P_v(0)\, g_v\right) \\ &+ T\sum_v P_v(0)\, g_v\ \left[\delta(q-q_v)\ \delta(q'-1)+\delta(q'-q_v)\ \delta(q-1)\right] \\ &+ \sum_v P_v(0)\, g_v \delta(q-q_v)\ \delta(q'-q_v) + \mathcal{O}(T^2) \end{aligned} \tag{4.22}$$

which yields that $P(q,q') = \frac{1}{3}P(q)\ \delta(q-q') + \frac{2}{3}\ P(q)\ P(q') + \mathcal{O}(T^2)$. Note that the sum rule is trivially satisfied at $T = 0$ if $P(q) = \delta(q-1)$. The important point here is that provided $P_v(0) > 0$, OPF remain finite for any system size at low temperature and the sum rule holds. Therefore, the numerator and denominator of G (3.5) remain finite and its ratio yields,

$$G = \frac{1}{3} + \mathcal{O}(T) \tag{4.23}$$

We can extend the same analysis to analyse A and B as well as the behaviour of the connected quantities A_c (3.10), G_c (3.11) and B_c (3.12) at low temperature. To perform the computations we need to calculate the distributions of three and four overlaps. For

the different moments of the connected overlaps we obtain,

$$\overline{\langle (q-\langle q\rangle)^k\rangle^m} = TP^{(1)}(0)\sum g_v f_{k,m}(v/V) + \mathcal{O}(T^2) \tag{4.24}$$

where $f_{k,m}(v)$ is a polynomial in v/V that depends on k and m. Thus, the outcome is that OPF are finite at order T provided there is a finite weight at zero cost. The analysis of the different terms yields that connected parameters have the following universal values at T_c, $G_c = 13/31$, $A_c \to \infty$ and $B_c \to -\infty$. The divergences in the two last parameters arise because both quantities have in the denominator the term $\left(\overline{\langle (q-\langle q\rangle)^2\rangle}\right)^2 \sim T^2$ that vanishes as a higher power of T than the numerator that contains only terms of the type (4.24) and, thus is linear in T. The same results are obtained if we consider only one-spin excitations, provided the local-field distribution has a finite weight at zero field.

We have already anticipated in Chap. 3 that the behaviour at low temperature of the parameter A (3.6) is related to the thermal exponent θ. Since the numerator is $\overline{\langle q^2\rangle}^2 = 1 + \mathcal{O}(T)$, the leading behaviour at low temperature (that is $\mathcal{O}(T)$) is given by the numerator,

$$\begin{aligned}\overline{\langle (q-\langle q\rangle)^2\rangle^2} &= \frac{16}{3}\frac{T}{V^4}\sum_v P_v(0)\, g_v\, v^2(v-V)^2 \\ &= \frac{1}{3}P^{(1)}(0)\, T\int dq\, g(q)\, \left(1-q^2\right)^2 \ . \end{aligned} \tag{4.25}$$

From what follows that in the low-temperature limit,

$$A \sim\ T\, L^{-\theta_l - d\lambda_l = -\theta}\ . \tag{4.26}$$

If $\theta > 0$, A vanishes at finite temperature implying that there is no RSB, and, if $\theta = 0$, A remains finite so that there is RSB. If $\theta < 0$, note that A diverges at finite temperature if we take the limit $V \to \infty$. However, we know that A must vanish at $T = 0$ for any system size. This is the typical situation encountered in a critical point where the correlation length diverges as we approach $T = 0$ as $\xi \sim T^{-\nu}$ so that the limits $T \to 0$ and $V \to \infty$ do not commute [10]. Therefore, θ is related to the correlation length exponent $\theta = -1/\nu$. This is the case of the EA model in one and two dimensions as we have seen in Secs. 3.1and 3.2

We conclude summarising our results. A low-T expansion for OPF reveals that the only condition to get $G = 1/3 + \mathcal{O}(T)$ and $A \sim TL^{-\theta}$ is that the ground state is unique and that the disorder average probability distribution for the lowest excitations is gap less and with finite weight at zero energy cost. This illustrates the importance of rare samples in determining the low-temperature properties of spin glasses. Moreover, we have argued

[10] This is exactly the same situation found in the spin glass susceptibility at order T, $\chi_{\rm SG} = V\overline{\langle q^2\rangle} \approx V\left(1 - \frac{4T}{V^2}\sum \mathcal{P}(v,\epsilon)\, v\,(V-v)\right) \sim V\left(1 - a\, T\, L^{-\theta}\right)$.

that the leading behaviour in T of any quantity can be described only by considering the lowest excitations. This is a very particular property of random systems with frustration which have gap-less rare excitations with a very small overlap with the ground state

In what follows we analyse the first excitations in mean-field models as well as short-ranged models to check the validity of our assumptions. In first place, we analyse the EA model in 1 and 2 dimensions which has a critical point at $T = 0$ so that we expect $\theta < 0$ and in second place a mean-field example: the SK model.

2. Lowest-lying excitations

2.1 The 1d Ising spin glass

An illustrative example of these results is the Ising spin-glass chain defined by the following Hamiltonian,

$$\mathcal{H} = -\sum_{i=1}^{V} J_i S_i S_{i+1}\,; \qquad S_i \pm 1 \tag{4.27}$$

where $V = L$ is the length of the chain and the quenched disorder is distributed according to some continuous distribution $P(J)$ with finite weight at zero coupling. The ground state is unique (up to a global spin inversion) and has an energy $E_{\rm GS} = -\sum_i J_i \sigma_i^* \sigma_{i+1}^*$. As we have already pointed out this model has a critical point at $T = 0$ with the correlation length diverging as $\xi \sim T^{-1}$. Therefore we read off $\theta = -1/\nu = -1$. In the study of the low-temperature excitations we have to distinguish between the cases with free and periodic boundary conditions.

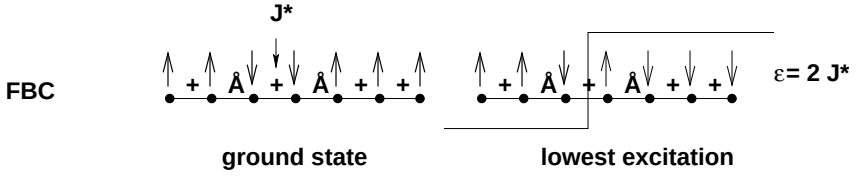

Figure 4.3. Lowest-lying excitation in the one-dimensional Ising chain with free boundary conditions. Each dot corresponds to a site and each line to a bond whose sign is indicated by $+$, $-$. Note that the ground-state configuration is not frustrated. The excitations with lowest energy correspond to breaking the weakest bond J^*.

In the free boundary case the minimum cost excitations correspond to breaking the weakest bond J^* and reversing all the spins on the right or left of that bond (see Fig. 4.3). The energy cost of such an excitation reads: $\epsilon = 2|J^*|$. Note that depending on the sample, the length of the droplet (v) can range between 1 an $L-1$ with equal probability yielding $g_v = 1/L$, thus small and large excitations yield the same contribution to the thermodynamics. From (4.9) it follows that $\lambda_l = 0$ and $\theta = \theta_l$. These excitations have a finite probability of having no energy cost that scales as $\hat{P}(\epsilon = 0) \sim L\, P(J^* = 0)$ so that

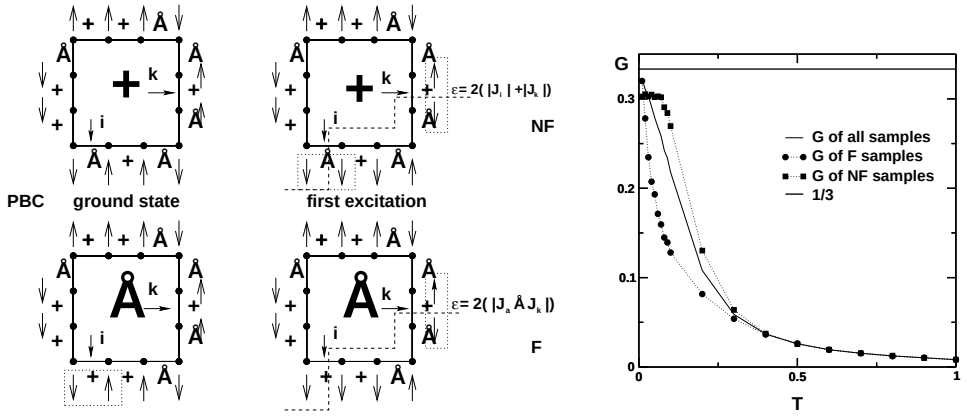

Figure 4.4. 1d Ising chain with PBC. *Left:* Here we represent it schematically as a closed square. We show an example of the ground state and the lowest excitation for a given realisation of the quenched disorder of a non-frustrated sample (NF-*top*) such that $\prod \mathrm{sign}[J_i] = +$ and a frustrated sample (F-*bottom*) such that $\prod \mathrm{sign}[J_i] = -$. The arrows point at the two weakest bonds J_i and J_k and the boxes show the unsatisfied couplings. Note that in the NF case there are two frustrated bonds (two boxes) in the lowest excitation whereas in the F samples the is only one frustrated bond. *Right:* We plot the parameter G corresponding to considering only F or NF samples as well as the G resulting from averaging over all the samples for $L = 1000$ and Gaussian couplings. Note that in the NF case G does not approach $1/3$ at $T = 0$ but that G corresponding to F samples as well as the total G do. This means that the leading behaviour to OPF at low temperature comes exclusively from F samples that have $P(\epsilon) > 0$.

$\theta = \theta_l = -d = -1$ as expected from the previous arguments and analytical results. Since this probability is finite by hypothesis, it follows that at $T = 0$ we obtain the universal value $G = 1/3$ in agreement with the analytical result derived in Sec. 3.1. Note that one-spin excitations cannot correspond to minimum cost excitations when considering spins which are not at the boundaries. This is due to the fact that, in this particular system, the ground state is not frustrated. Exciting one interior spin would necessarily frustrate two bonds so that the energy cost would be: $\epsilon^* = 2(|J_i| + |J_k|)$, which is obviously less favourable than breaking a single bond. It is easy to check that $g_v = \frac{1}{L}$ substituted in (4.25) yields $A = \frac{8P(0)T(L^4-1)}{45L^3}$ in full agreement with the result obtained with transfer matrix calculations in the preceding chapter (3.60).

For periodic boundary conditions, the excitations are different but the considerations for the scaling of the probability distributions still hold. Here we have L spins and L couplings, with the condition $\sigma_{L+1} = \sigma_1$. Note that the ground state can have frustrated bonds, so that we can distinguish between two different kinds of samples: non-frustrated (NF) having $\prod_i \mathrm{sign}[J_i] = +$ and frustrated (F) having $\prod_i \mathrm{sign}[J_i] = -$. In the first case the ground-state energy reads: $E^*_{\mathrm{NF}} = -\sum_i |J_i|$ while in the second we have that the weakest bond, let us say J_k, is unsatisfied so that the ground-state energy reads: $E^*_{\mathrm{F}} = E^*_{\mathrm{NF}} + 2|J_k|$ as is schematised in Fig. 4.4. In both cases, the minimum energy

excitation will correspond to breaking the two weakest bonds, let's say (i,k), but the energy cost will read differently in each case: $\epsilon_{\rm NF} = 2(|J_i| + |J_k|), \epsilon_{\rm F} = 2(|J_i - J_k|)$. From here, it is evident that the energy gap in the F set will be much smaller than in the NF set. Thus, only F samples yield contributions $\mathcal{O}(T)$ at low temperature. This has been numerically checked by transfer matrix calculations. F samples yield $G = 1/3$ at $T = 0$ while NF samples yield a lower value of G at $T = 0$ as we can see in the right panel in Fig. 4.4. In other words, $\hat{P}(\epsilon_{\rm F} = 0) \neq 0$ while $\hat{P}(\epsilon_{\rm NF} = 0) = 0$ although, in average, still $G(T = 0) = 1/3$ and $A \sim TL$.

We have see in the previous chapter that the scaling TV for G and A goes further beyond the region of validity of the lowest excitation $T < V^{-1}$. As a matter of fact the same situation is met in the spin glass susceptibility which can be expressed in terms of a scaling function $\chi_{\rm SG}(T,V) = V\,\hat{\chi}(TV)$, such that at finite temperature is analytical in TV but that in the thermodynamic limit $\hat{\chi}$ vanishes at low temperature except at $T = 0$ where $\chi_{\rm SG}$ diverges $\sim V$. Because $\lambda_l = 0$, at order T^p all the excitations at different levels yield the same dominant contributions proportional to some power of $TL^{-\theta=-\theta_l}$ as well as we found for the specific heat.

Indeed, the validity of the previous arguments can be checked as well for the specific heat which can be computed analytically in the FBC case. Starting from the partition function $\mathcal{Z} = 2\left(2^{V-1}\prod_i \cosh(\beta J_i)\right)$ [BM85], because all the J_i are independent random variables we immediately obtain that the specific heat reads,

$$\begin{aligned} c &= \beta^2 \int_0^\infty dJ\, P(J)\, \left(\frac{J}{\cosh(\beta J)}\right)^2 \\ &\overset{\beta\to\infty}{\to} TP(0)\int_0^\infty dx \left(\frac{x}{\cosh(x)}\right)^2 = \frac{\pi^2}{12} TP(0) + \mathcal{O}(T^2)\ . \end{aligned} \tag{4.28}$$

So that c vanishes linearly in T at all *finite* volumes and thus we recover the first term in the expansion for c in (4.15).

2.2 The 2d Ising spin glass

In this section we address the two-dimensional Ising spin glass with Gaussian coupling defined by the following Hamiltonian,

$$\mathcal{H} = -\sum_{\langle i,j\rangle} J_{ij} S_i S_j \qquad S_i \pm 1\ . \tag{4.29}$$

As well as the 1d model, this model has a transition at $T = 0$. However, the case of the 2d spin glass is more complex. Since there is no analytical solution we have to rely on the numerical approach. However, finite-size effects are very large so that a consensual description of the excitations relevant close to $T = 0$ is difficult to establish.

Numerical details: We have analysed the EA model in $d = 2$ in squared lattices of size L with a Gaussian distribution of the couplings. We have numerically computed the ground states and the

first and second lowest-lying excitations. We have used squared lattices of linear size $L = 5 - 11$ with PBC along both directions (PP), and also with free-boundary conditions along one (PF) or both directions (FF) for even sizes $L = 6 - 16$ obtaining the same results. The number of samples used is larger than $ns = 1000000$ for every lattice size. The numerical algorithm that has been used is described in appendix C. In the study of the specific heat at low temperature we have studied PP lattices sizes $L = 3 - 8$ with 100000 samples for each lattice size. For the smallest sizes $L = 3, 4$ we have exactly enumerated the partition function and for the larger ones we have used the finite temperature transfer matrix method.

The analysis of the lowest-lying excitations reveals that $\lambda_l > 0$ so that $\theta \neq \theta_l$. Moreover, finite-size corrections to θ_l and λ_l are very large in this model. Therefore we have made the analysis in terms of *effective exponents* $(\lambda_l^{\rm eff}(L),\ \theta_l'^{\rm eff}(L))$ that describe the energy and volume distributions at a given lattice size L. Despite, the estimation obtained for the thermal exponent, $\theta = -0.48$ is in agreement with results found in the literature obtained by MC simulations. Furthermore, we have analysed also the statistics of the second lowest-lying excitations to find that the assumptions made in the random energy scenario hold. And in particular we have been able to test the scaling behaviour of the specific heat proposed in Sec. 1.1.

- Volume distribution
  In Fig. 4.5 we show the $g(q) = \frac{2}{V} g_v$ versus $1 - q$ for the PP and FF cases. Note that there are excitations of all sizes but that one-spin excitations dominate over all other excitations. As a matter of fact, less than the 10% of the samples have large excitations with q in the range $0 - 0.5$. Remarkably all the distribution is described by a single scaling exponent $\lambda_l^{\rm eff}$ which is roughly the same for the cases (PP, FF and PF) and sizes studied. One can nicely interpolate between the power-law divergence at $q = 1$ with the flat tail at $q = 0$, by proposing the following functional form of the $g(q)$ [11],

$$g(q) = \frac{1}{2V^{\lambda_l}} \left(a + \frac{b}{(1-q)^{\lambda_l + 1}} \right) \tag{4.30}$$

  where a and b are constants that have to fulfil the normalisation condition $(a - b\lambda_l^{-1})(2V^{\lambda_l}) + b/(2^{\lambda_l+1}\lambda_l) = 1$ [12]. Certainly we should carry out an independent fit for every size to obtain $a, b, \lambda_l^{\rm eff}$. However, we can obtain an independent estimate of $\lambda_l^{\rm eff}$ from the average volume. From previous considerations it can be assumed to behave as $\overline{v} = c + dV^{1-\lambda_l}$ which yields a best fit value of $\lambda_l^{\rm eff} = 0.7 \pm 0.05$. In the insets of both panels in Fig. 4.5 we plot the scaling function $V^{\lambda_l} g(q)$ for different sizes with this effective value. We have to point out that there are systematic corrections with size to the best fitting values in (4.30) which means that larger sizes scale better than smaller ones, but still the scaling is remarkably good.

[11] Note that there is no strict divergence of the $g(q)$ because $q \leq 1 - 2/V$, as the smallest excitation corresponds to $v = 1$.

[12] This constants can be numerically evaluated fitting the $g(q)$ in Fig. 4.5 with (4.30) obtaining in the PPBC case $a = 1.55 \pm 0.03$ and $b = 0.777 \pm 0.003$.

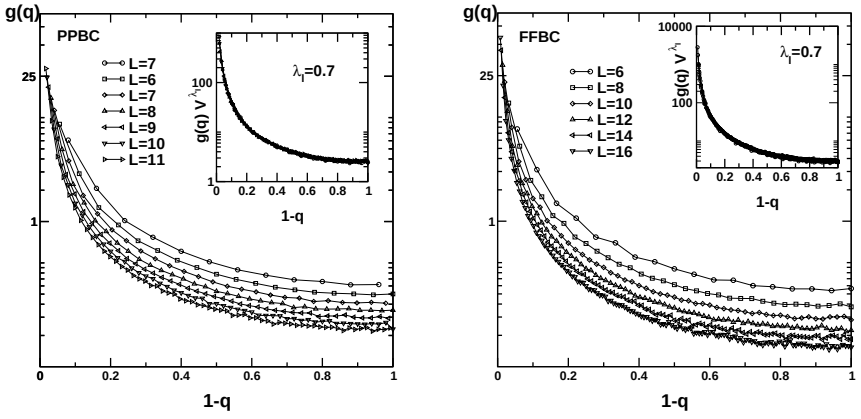

Figure 4.5. Volume distribution of the 2d spin glass. We plot $g(q)$ versus $1-q$ for different lattice sizes *Left:* PP boundary conditions $L = 5 - 11$. *Right:)* FF boundary conditions $L = 6 - 16$. In the insets we plot the scaling function $\hat{g}(q) = V^{\lambda_l^{\rm eff}} g(q)$ with the same effective parameter $\lambda_l^{\rm eff} = 0.7$.

- Energy distribution
  In the left panel in Fig. 4.6 we show the results for the energy gap distributions. As assumed in the random energy level scenario, we show in inset b) that the $P_v(\epsilon)$'s do not depend on the excitation size. Thus, we can assume that the distribution of all energy costs $P^{(1)}(\epsilon)$ satisfies the following scaling ansatz $P^{(1)}(\epsilon) = L^{-\theta_l} \hat{P}(\epsilon L^{-\theta_l})$. The scaling function shown in inset a) is to a very good approximation an exponential (and thus with finite weight at zero gap). However, we find that there are strong sub-dominant correction to the thermal exponent. The best data collapse shown in inset a) corresponds to $\theta_l^{\rm eff} = -1.7 \pm .1$ which is very far from the expected value $\theta_l^{\rm eff} = -2$.

- θ exponent
  The systematic correction with size to λ_l and θ_l make it difficult to give a precise estimation of $\theta = \theta_l + d\lambda_l$. The most accurate procedure is to construct observables from which θ can be directly evaluated. This is the case for instance of parameter A that vanishes as $TL^{-\theta}$. As shown in Fig. 3.17 the scaling of different sizes in the linear regime yields $\theta = -0.46$. A more systematic analysis has been performed on the following observable,

$$Q(L) = \frac{V\overline{\epsilon}(L)}{\overline{v}(L)} \sim \frac{L^d\, L^{\theta_l}}{L^{d(1-\lambda_l)}} \sim L^{\theta} \ . \tag{4.31}$$

  At a given L we can estimate θ from the fit of $Q(L')$ for L' in the range $[L, L_{\max} = 11]$. The estimates of θ are independent of L, since we obtain that for $L = 4, 6, 9$ the following values for $\theta(L) : (L = 4) - 0.460 \pm 0.001$, $(L = 6) - 0.462 \pm 0.002$ and $(L = 9) - 0.459 \pm 0.02$. Note that in the last estimation, the large error bars are due

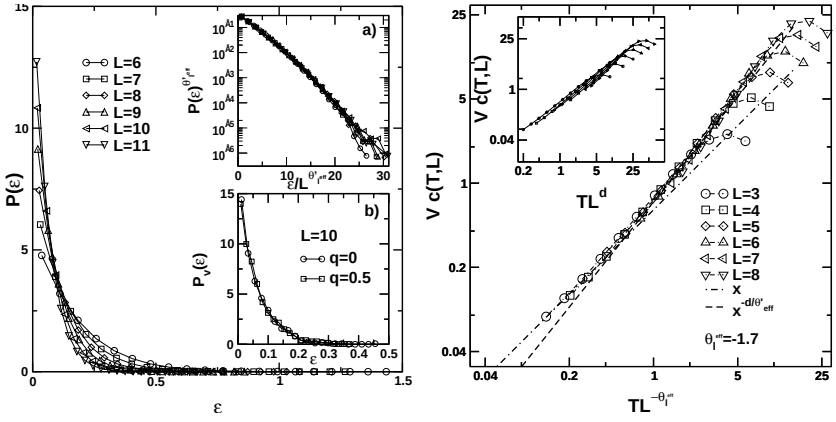

Figure 4.6. *Left:* Energy cost distribution $P(\epsilon)$ versus ϵ for different lattice sizes in the PP case. In inset a) we plot the scaling function $\hat{P}(\epsilon) = P(\epsilon)L^{\theta_l^{\rm eff}}$ versus the scaling variable $\epsilon L^{-\theta_l^{\rm eff}}$ with the effective parameter $\theta_l^{\rm eff} = -1.7$. In inset b) we show $P_v(\epsilon)$ for different excitation sizes $q = 0, 0.5$. *Right:* Heat capacity $C(T,L) = Vc(T,L)$ versus the scaling variable $TL^{-\theta_l^{\rm eff}}$, with $\theta_l^{\rm eff} = -1.6$. In the inset, we plot the heat capacity versus the expected scaling variable TV corresponding to $\theta_l = -d = -2$.

to the fact that the maximum size studied is $L = 11$. Thus it appears that the strong corrections to the lowest-droplet exponent seem to cancel out to yield a rather constant value θ (see Fig. 4.7). This estimate is in agreement with Monte Carlo or transfer matrix estimates $\theta = -.48(1)$ but is certainly smaller than DW reults $\theta_{\rm DW} = -.285$ (see [HY02] for a collection of different estimates).

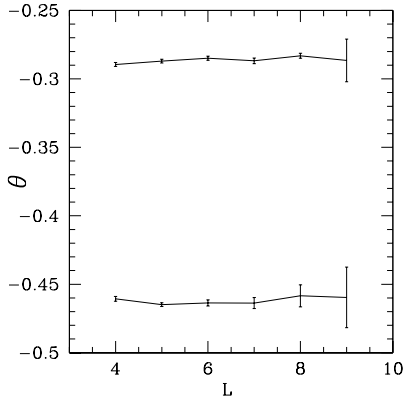

Figure 4.7. DW exponent (*top*) and θ exponent computed as explained in the text versus L. Note that both exponents different and rather constant for the sizes.

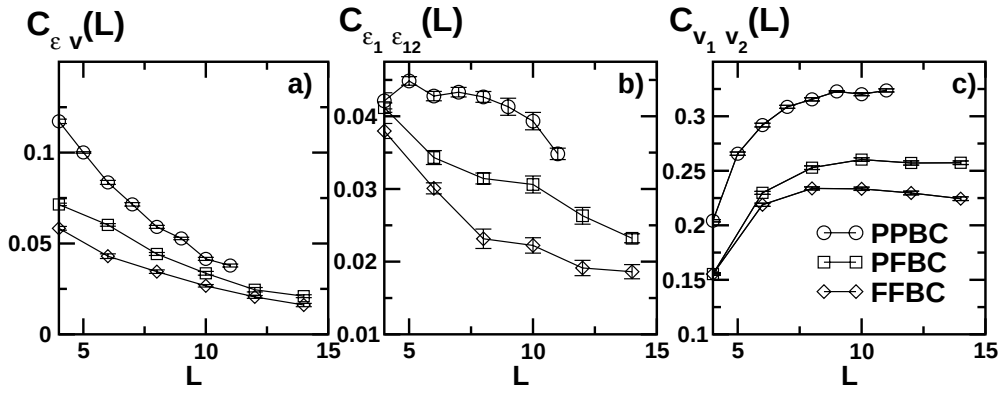

Figure 4.8. Correlation functions in the 2d Ising spin glass versus lattice size for the three cases under study (PP, PF and FF). *Plot a)* $C_{\epsilon v}(L)$: cross-correlation between the energy gap and the volume of the first excitation. *Plot b)* $C_{\epsilon_1,\epsilon_{12}}(L)$: correlation between energy gaps ϵ_1 and $\epsilon_{12} = \epsilon_2 - \epsilon_1$ of the same sample. *Plot c)* $C_{\epsilon_1,\epsilon_{12}}(L)$: correlation between excitation volumes v_1 and v_2 of the same sample.

- Correlations and the Specific Heat

  We have also studied the statistics of the second lowest-lying excitations to obtain similar results. In order to check the degree of correlation between different excitations, given two observables x, y that can be either gaps or volumes, we have built the following correlation functions,

$$c_{x,y}(L) = \frac{\overline{x\,y} - \overline{x}\,\overline{y}}{\sqrt{\overline{(x-\overline{x})^2}}\,\sqrt{\overline{(y-\overline{y})^2}}} \tag{4.32}$$

  In Fig. 4.8 we show in plot a) the correlations between the gap and volume of the first excitations; in plot b) the correlations between gaps ϵ_1 and ϵ_{12}, where ϵ_{12} is the gap between the first and the second excitation; and in plot c) the correlations between volumes of first and second excitations. The result is that for all the cases under study the correlations between gaps and the correlation between gaps and volumes vanish in the large L limit. This is not the case of the excitation volumes, whose correlations do not have a tendency to decrease within the sizes analysed.

  Since all the previous hypothesis on the energy gap distribution hold in this model, the behaviour of the specific heat must reflex the scaling properties derived in Sec. 1.1. In particular, we expect that the heat capacity $C(T,L) = V\ c(T,L)$ is a scaling function of the variable $x \sim TL^{-\theta_l^{\rm eff}}$, displaying a crossover from the linear behaviour for small x to the power law behaviour $\sim x^{-d/\theta_l^{\rm eff}}$ in the large x limit. In the right panel in Fig. 4.6 we plot precisely this scaling function for lattice sizes $L = 3, 8$ together with the two limiting behaviours. The agreement with the theoretical predictions is remarkable. Note that the collapse of the data with $\theta_l = -2$ would not be good at

all (see inset in Fig. 1.2. We have also to point out that in the one-dimensional case with FBC there are no finite-size corrections to the energy exponent $\theta_l = -1$ and the specific heat in (4.28) is linear for any V. This is because the weight at zero energy cost depends on the weight at zero coupling, $\mathcal{P}(0) \sim V\ P(J=0)$, which, by definition, is independent of system size. Nevertheless, finite-volume corrections to $\theta_l = -1$ would be present in the PBC case. In the latter, the energy distribution of the lowest excitations with no gap corresponds to $P(|J_i - J_j)$ where $J_{i/j}$ are the weakest bonds, and we expect it to have finite size corrections.

2.3 Mean-field first excitations: the SK model

In this section we analyse the lowest excitations of the SK model. This model has a low-temperature solution where replica symmetry is broken, thereby we expect that the analysis of lowest-lying excitations yields $\theta = 0$. We have to point out that excitations in mean-field models do not have topology because all spins interact with each other. Therefore, we cannot define a linear size of the system and we have to work in terms of system volumes. For this reason, we rewrite the scaling ansatz for the energy gap distributions by introducing a lowest-droplet exponent for MF excitations that we denote $\Theta_l = \theta_l/d$ such that,

$$P_v(\epsilon) = V^{-\Theta_l} \hat{P}_v \left(\frac{\epsilon}{V^{\Theta_l}} \right) \quad . \tag{4.33}$$

In the same way we redefine the thermal exponent θ for mean-field excitations $\Theta = \Theta/d$, so that $\Theta = \Theta_l + \lambda_l$. With this definitions, from expression (4.15) the specific heat at low temperature vanishes as $c \sim T^{-1/\Theta_l}$ and from (4.19) the contribution to the $P(q)$ coming from large size excitations at finite temperature scales as $\sim T\, V^{-\Theta}$.

In the following analysis we show that from the statistics of the lowest-lying excitations many properties about the low-temperature phase can be inferred even from the study of small samples. The study of OPF parameters presented in the previous chapter reveals that the analysis of small samples yields the relevant information about the infinite-volume behaviour. The estimates for Θ_l and λ_l are not so affected by finite-size corrections as compared to the two-dimensional model studied before.

2.3.1 The SK model

The SK model has been widely studied but the lowest-lying excitations have never been explored. We have studied the energy and volume distributions of small system sizes through the scaling ansätze proposed for $P_v(\epsilon)$ (4.33) and g_v (4.9). The numerical estimate yield by the average energy cost and volume excitation yields $\Theta_l^{\text{eff}} = -0.54 \pm .04$ and $\lambda_l^{\text{eff}} = 0.51 \pm 0.02$ so that $\Theta = -0.03 \pm 0.04$ which is well compatible with zero, the expected value.

Numerical Details: We have computed numerically the exact ground states, first excited states of the SK model with Gaussian disorder for small samples $V = 8, 10, 11, 13, 18$ by enumerating all the configurations. The number of samples is very large, from 10^6 for the smallest sizes to 300000 for the largest one.

The properties of the lowest-lying excitations are different to those observed for the EA model in $d = 1, 2$. The main difference concerns the energy-cost distributions, because the distribution depends on the size of the excitation. At least for the sizes studied we find that the gap distribution of one-spin excitations is different to the gap distribution of larger size excitations ($v > 1$). This difference is clearly illustrated in Fig. 4.9 where, in the inset b) of the right panel, we plot energy distributions at fixed overlap. In the left panel we plot the distribution of energy costs corresponding to one-spin excitations ($q = 1 - 2/V$) for different volumes. And in the right one, we show the gap distribution of excitations whose overlap with the ground state is zero ($v = V/2$). In the inset b) of the right panel we show the distribution of gaps at fixed volume $v = 1, 2, V/4, V/2$ for the largest system size analysed $V = 18$. Note that $P_{v=1}(\epsilon)$ is very different from $P_{v>1}(\epsilon)$.

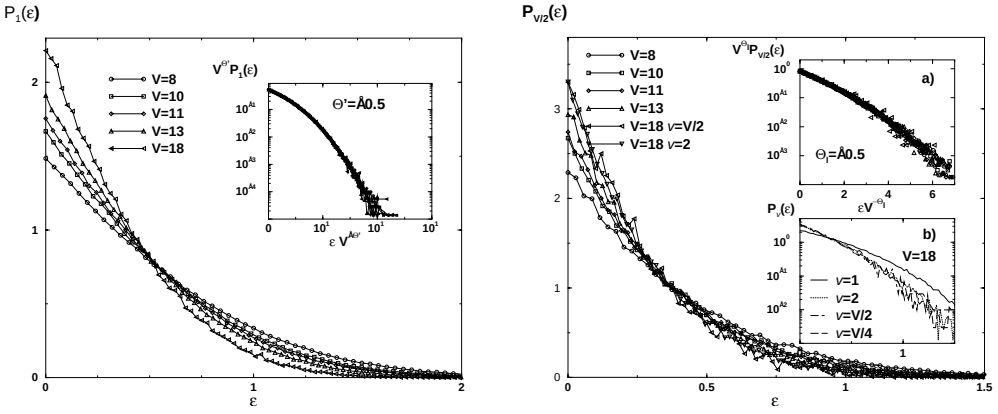

Figure 4.9. Energy distributions of the lowest-lying excitations *Left:* Distribution of energy gaps of one-spin excitations for different sizes. In the inset we plot the scaling function $\hat{P}_1(\epsilon/V^{\Theta_l}) = V^{\Theta_l} P_1(\epsilon)$ versus the scaling variable $\epsilon V^{-\Theta_l}$ with $\Theta_l = -0.5$. *Right:* Distribution of energy gaps of system size excitations with $v = V/2$. Note that the distribution for system size excitations coincide, but are different from the one-spin gap distribution. In inset a) we plot the scaling function with $\Theta = -0.5$. In inset b) we show the $P_v(\epsilon)$ for the largest size $V = 18$ for excitation volumes $v = 1, 2, V/4$ and $V/2$. Note that the dotted ($v = 2$), dashed ($v = V/4$) and long-dashed ($v = V/2$) lines can hardly be distinguished whereas the solid line ($v = 1$) has a very different shape.

Nevertheless, all the distributions scale with the same exponent $\Theta_l = -0.5$ as we can see in the top insets of both panels. This is the exponent that we can derive from the local-field distribution at the ground state $P(h_{\rm loc})$ [13]. The local-field distribution of the SK model has been well studied and in the thermodynamic limit vanishes $\sim h$, when

[13] Note that this holds in the case that the whole distribution is self-averaging. We have checked numerically this assumption by looking at the fluctuations of the local-field distribution through the quantity $\overline{\langle h_i^2 \rangle^2} - \overline{\langle h_i^2 \rangle}^2$ which decreases with system size as in short-ranged systems.

$h \to 0$. From previous arguments we know that if the local-field distribution vanishes in the infinite-volume limit as a power law with exponent η, the average gap of the lowest one-spin excitation scales as $\sim V^{-1/(\eta+1)}$. Consequently $\Theta_l = -1/(\eta+1)$, so that in this particular case $\eta = 1$ which yields $\Theta_l = -0.5$ [14] . This is exactly the exponent that we have used in the scaling plots in Fig. 4.9 with quite good results.

We have seen that we have two different energy distributions, one for one-spin excitations and one for larger sizes, but we expect this difference to disappear for larger system volumes. Nonetheless, since large excitations have exactly the same statistics the predictions made in the random-energy level scenario are not affected, because the value obtained for $\Theta_l^{\rm eff}$ yields that the specific heat vanishes as $c \sim T^2$ in agreement with the exact computations [MPV87].

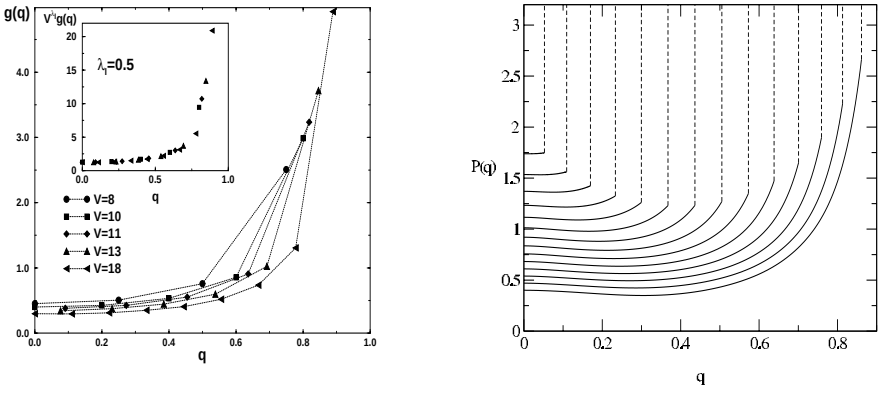

Figure 4.10. Volume distribution of the lowest-lying excitations of the SK model. *Left:* Volume distribution of the first excitations $g(q) = \frac{V}{2} g_v$ versus $1-q$ for different system sizes. In the inset we plot the scaling function $\hat{g}(q) = V^{\lambda_l} g(q)$ with $\lambda_l = 0.5$. *Right:* Exact $P(q)$ computed numerically computed for temperatures $T = .95$ to $T = .3$ by A. Crisanti and T. Rizzo in [CR02a].

The distribution of excitation volumes is shown in the left panel of Fig. 4.10. In the inset we show the scaling function $\hat{g}(q) = V^{\lambda_l} g(q)$ versus q with $\lambda_l = 0.5$ as obtained from the fit of the average excitation volume $\overline{v} \sim V^{1-\lambda_l}$. Note that the scaling is very good. Combining this result for λ_l with the value obtained for Θ_l we get that $\Theta = 0$. Thus we expect that there the $\hat{g}(q)$ contains the same information as the $P(q)$ at low temperature. Indeed, the comparison with the $P(q)$ in the infinite-volume limit computed numerically by Crisanti and Rizzo in [CR02a] shown in Fig. 4.10 is very similar, corroborating the predictions presented above.

[14] The $P(0)$ is finite for a finite system size and vanishes $\sim 1/\sqrt{V}$ [PZZ99]. Therefore from the condition $V P_1(0) h^* \sim 1$ read off $\epsilon \sim h^* \sim 1/\sqrt{V}$, and thereby $\Theta_l^{\rm eff} = -0.5$.